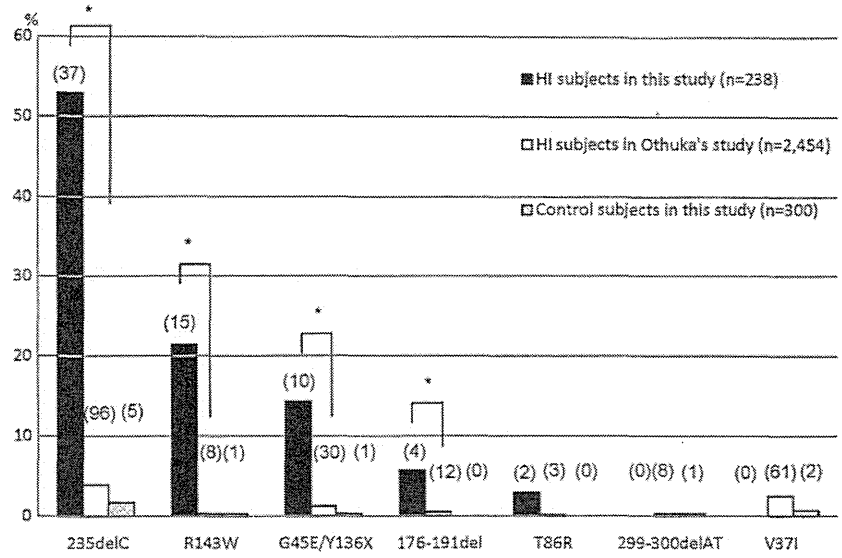

Fig. 1. Allele frequency for each mutation in three groups. A Z-test was used to assess the difference in frequency. Note the *P*-value of <0.01 between the two deafness groups for c.235delC, p.R143W, p.G45E/Y136X, and c.176-191del. *$P < 0.01$.

(p.R32S and p.P225L) are highly conserved among various species, and we did not detect any of these mutations in 300 chromosomes in normal Japanese controls.

4. Discussion

In this study, *GJB2*-related deafness patients accounted for 29.4% of non-syndromic deafness cases. This frequency was less than in a previous report, which pointed to a frequency of around 50% [6]. Familial cases were twice as prevalent as sporadic cases. In most of the previously reported studies, the prevalence of *GJB2* mutations was significantly higher in familial non-syndromic deafness than in sporadic cases [7,26,27]. The frequent mutations of *GJB2* (c.235delC, p.R143W, p. G45E/Y136X, and c.176-191del) in this study were partly different from previous reports [25]. It is assumed that all of our subjects had severe to profound deafness, as they had received cochlear implants, whereas Ohtsuka's subjects had mild to profound deafness and included heterozygous mutations. A few studies have confirmed that some genotypes are correlated with clinical phenotypes in *GJB2*-related deafness. Further, truncating mutations are associated with a greater degree of deafness than non-truncating mutations [9,21,22]. For this reason, three of these cases might be truncating mutations. In contrast, p.R143W mutation was previously implicated in an extraordinarily high prevalence of profound deafness in Ghana [15,28] and Caucasians [9]. This missense mutation may also show an important correlation with severe deafness in Japan. On the other hand, an effect of geography on the allele frequency may have been present, because most of our subjects were from a different area compared to a previous report [25].

The relation between p.V37I mutation of *GJB2* and SNHL is controversial. While some reports suggest that this mutation is

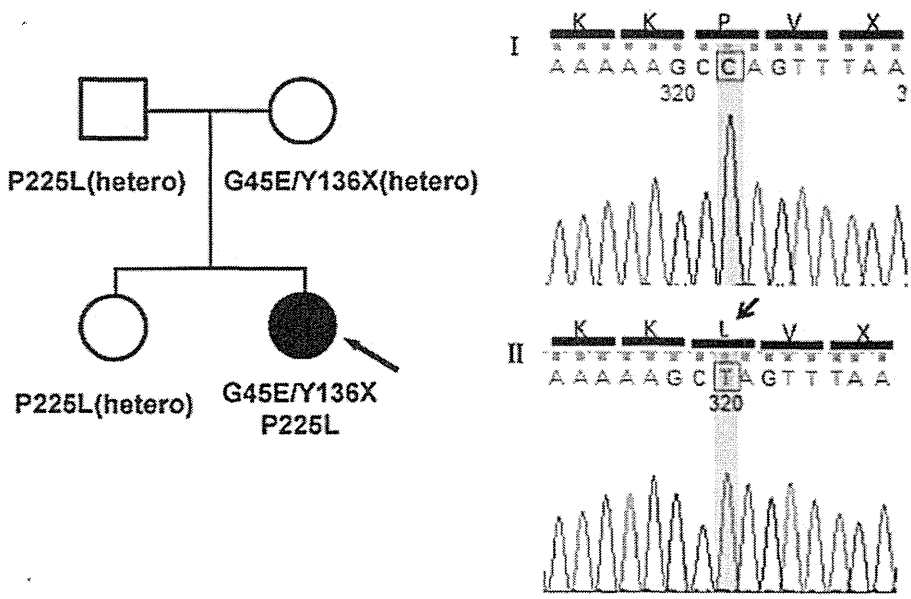

Fig. 2. (A) The pedigree and PCR direct sequencing results for the family; the arrow indicates the proband. (B) The sequencing results on TA cloning. Genomic PCR products were subcloned into a plasmid vector and sequenced separately (see Section 2). The sequences from independent clones are shown in the above two examples. I shows wild-type sequence, whereas II shows mutated sequence in which the proline residue is changed to leucine. Three of 8 subclones showed a missense mutation similar to that in II.

more common among individuals of Asian ancestry [11,12,29], others suggest that homozygous p.V37I is associated with slight/mild hearing loss [22,30,31]. In this study, no cases of homozygous p.V37I were observed. These findings support that this mutation is associated with mild hearing loss, because all of our subjects showed severe deafness.

The two unreported *GJB2* mutations, p.R32S and p.P225L, were not detected in normal hearing controls. These appeared in amino acid residues that were highly conserved. Additionally, three types of mutation were seen in arginine as the thirty-second amino acid, such as p.R32C, p.R32L, and p.R32H. Therefore, R32 is thought to be a mutation "hot spot." Thus, it is likely that these are pathological mutations, rather than rare or functionally neutral polymorphic changes. On the other hand, the mutation site of p.P225 located at the C-terminus of Connexin26 has not previously been reported. As the C-terminus region of connexins is thought to be an important region for intracellular molecular signaling and interaction with scaffolding proteins and the cytoskeleton [32–34], p.P225L mutation found in this study may affect important intracellular molecular networks to maintain the normal function of the cochlear gap junction.

5. Conclusion

In conclusion, this study identified significant genotypic features of Japanese children with profound non-syndromic deafness. Further research is required covering a broader range of genes in the subjects in this study with either single heterozygous or no mutation, in order to better understand the epidemiology of deafness in Japan.

Acknowledgements

We thank all the subjects who participated in the present study. We also thank Ms. Naoko Tamura and Ms. Tomoko Kataoka (Tokyo Medical University School of Medicine), for recruiting families with non-syndromic deafness, and Ms. Junko Onoda (Juntendo University School of Medicine) for assisting in our experiments.

References

[1] A.C. Davis, The prevalence of deafness and reported hearing disability among adults in Great Britain, Int. J. Epidemiol. 18 (1989) 911–917.
[2] D.H. Wilson, P.G. Walsh, L. Sanchez, The epidemiology of deafness in an Australian adult population, Int. J. Epidemiol. 28 (1999) 247–252.
[3] N.E. Morton, Genetic epidemiology of deafness, Ann. N. Y. Acad. Sci. 630 (1991) 1631.
[4] M.L. Marazita, L.M. Ploughman, B. Rawlings, E. Remington, K.S. Arnos, W.E. Nance, Genetic epidemiological studies of early-onset deafness in the U.S. school-age population, Am. J. Med. Genet. 46 (1993) 486–491.
[5] V. Kalatzis, C. Petit, The fundamental and medical impacts of recent progress in research on hereditary hearing loss, Hum. Mol. Genet. 7 (1998) 1589–1597.
[6] A. Kenneson, K. Van Naarden Braun, C. Boyle, GJB2 (connexin 26) variants and nonsyndromic sensorineural hearing loss: a HuGE review, Genet. Med. 4 (2002) 258–274.
[7] F. Denoyelle, S. Marlin, D. Weil, L. Moatti, P. Chauvin, E.N. Garabedian, et al., Clinical features of the prevalent form of childhood deafness, DFNB1, due to a connexin-26 gene defect: Implications for genetic counselling, Lancet 353 (1999) 1298–1303.
[8] A. Murgia, E. Orzan, R. Polli, M. Martella, C. Vinanzi, E. Leonardi, et al., Cx26 deafness: mutation analysis and clinical variability, J. Med. Genet. 36 (1999) 829–832.
[9] R.L. Snoeckx, P.L. Huygen, D. Feldmann, S. Marlin, F. Denoyelle, J. Waligora, et al., *GJB2* mutations and degree of hearing loss: a multicenter study, Am. J. Hum. Genet. 77 (2005) 945–957.
[10] Y. Fuse, K. Doi, T. Hasegawa, A. Sugii, H. Hibino, T. Kubo, Three novel connexin26 gene mutations in autosomal recessive non-syndromic deafnesss, Neuro Report 10 (1999) 1853–1857.
[11] S. Abe, S. Usami, H. Shinkawa, P.M. Kelley, W.J. Kimberling, Prevalent connexin 26 gene (*GJB2*) mutations in Japanese, J. Med. Genet. 37 (2000) 41–43.
[12] T. Kudo, K. Ikeda, S. Kure, Y. Matsubara, T. Oshima, K. Watanabe, et al., Novel mutations in the connexin 26 gene (*GJB2*) responsible for childhood deafness in the Japanese population, Am. J. Med. Genet. 90 (2000) 141–145.
[13] H.J. Park, S.H. Hahn, Y.M. Chun, K. Park, H.N. Kim, Connexin 26 mutations associated with nonsyndromic hearing loss, Laryngoscope 110 (2000) 1535–1538.
[14] P. Gasparini, R. Rabionet, G. Barbujani, S. Melchionda, M. Petersen, K. Brondum-Nielsen, et al., High carrier frequency of the 35delG deafness mutation in European populations, Genetic Analysis Consortium of GJB2 35delG, Eur. J. Hum. Genet. 8 (2000) 19–23.
[15] G.W. Brobby, B. Muller-Myhsok, R.D. Horstmann, Connexin 26 R143W mutation associated with recessive nonsyndromic sensorineural deafness in Africa, N. Engl. J. Med. 338 (1998) 548–550.
[16] M. Maheshwari, R. Vijaya, M. Ghosh, S. Shastri, M. Kabra, P.S. Menon, Screening of families with autosomal recessive non-syndromic hearing impairment (ARNSHI) for mutations in GJB2 gene: Indian scenario, Am. J. Med. Genet. A 120A (2003) 180–184.
[17] M. RamShankar, S. Girirajan, O. Dagan, H.M. Ravi Shankar, R. Jalvi, R. Rangasayee, et al., Contribution of connexin26 (GJB2) mutations and founder effect to non-syndromic hearing loss in India, J. Med. Genet. 40 (2003) e68.
[18] G. Minárik, V. Ferák, E. Feráková, A. Ficek, H. Poláková, L. Kádasi, High frequency of GJB2 mutation W24X among Slovak Romany (Gypsy) patients with non-syndromic hearing loss (NSHL), Gen. Physiol. Biophys. 22 (2003) 549–556.
[19] P. Seeman, M. Malíková, D. Rasková, O. Bendová, D. Groh, M. Kubálková, et al., Spectrum and frequencies of mutations in the GJB2 (Cx26) gene among 156 Czech patients with pre-lingual deafness, Clin. Genet. 66 (2004) 152–157.
[20] A. Alvarez, I. del Castillo, M. Villamar, L.A. Aguirre, A. González-Neira, A. López-Nevot, et al., High prevalence of the W24X mutation in the gene encoding connexin-26 (GJB2) in Spanish Romani (gypsies) with autosomal recessive non-syndromic hearing loss, Am. J. Med. Genet. A 137A (2005) 255–258.
[21] K. Cryns, E. Orzan, A. Murgia, P.L. Huygen, F. Moreno, I. del Castillo, et al., A genotype-phenotype correlation for *GJB2* (connexin 26) deafness, J. Med. Genet. 41 (2004) 147–154.
[22] T. Oguchi, A. Ohtsuka, S. Hashimoto, A. Oshima, S. Abe, Y. Kobayashi, et al., Clinical features of patients with *GJB2* (connexin 26) mutations: Severity of hearing loss is correlated with genotypes and protein expression patterns, J. Hum. Genet. 50 (2005) 76–83.
[23] K. Fukushima, K. Sugata, N. Kasai, S. Fukuda, R. Nagayasu, N. Toida, et al., Better speech performance in cochlear implant patients with GJB2-related deafness, Int. J. Pediatr. Otorhinolaryngol. 62 (2002) 151–157.
[24] F.J. Del Castillo, M. Rodríguez-Ballesteros, A. Alvarez, T. Hutchin, E. Leonardi, C.A. de Oliveira, et al., A novel deletion involving the connexin-30 gene, del(*GJB6*-d13s1854), found in trans with mutations in the *GJB2* gene (connexin-26) in subjects with DFNB1 non-syndromic deafnesss, J. Med. Genet. 42 (2005) 588–594.
[25] A. Ohtsuka, I. Yuge, S. Kimura, A. Namba, S. Abe, L. Van Laer, et al., *GJB2* deafness gene shows a specific spectrum of mutations in Japan, including a frequent founder mutation, Hum. Genet. 112 (2003) 329–333.
[26] J. Loffler, D. Nekahm, A. Hirst-Stadlmann, B. Gunther, H.J. Menzel, G. Utermann, et al., Sensorineural hearing loss and the incidence of Cx26 mutations in Austria, Eur. J. Hum. Genet. 9 (2001) 226–230.
[27] A. Pampanos, J. Economides, V. Iliadou, P. Neou, P. Leotsakos, N. Voyiatzis, et al., Prevalence of *GJB2* mutations in prelingual deafness in the Greek population, Int. J. Pediatr. Otorhinolaryngol. 65 (2002) 101–108.
[28] C. Hamelmann, G.K. Amedofu, K. Albrecht, B. Muntau, A. Gelhaus, G.W. Brobby, et al., Pattern of connexin 26 (*GJB2*) mutations causing sensorineural deafness in Ghana, Hum. Mutat. 18 (2001) 84–85.
[29] WangYC, C.Y. Kung, M.C. Su, C.C. Su, H.M. Hsu, C.C. Tsai, et al., Mutations of Cx26 gene (*GJB2*) for prelingual deafness in Taiwan, Eur. J. Hum. Genet. 10 (2002) 495–498.
[30] C. Huculak, H. Bruyere, T.N. Nelson, F.K. Kozak, S. Langlois, V37I connexin 26 allele in patients with sensorineural hearing loss: Evidence of its pathogenicity, Am. J. Med. Genet. A 140 (2006) 2394–2400.
[31] H.H. Dahl, K. Saunders, T.M. Kelly, A.H. Osborn, S. Wilcox, B. Cone-Wesson, et al., Prevalence and nature of connexin 26 mutations in children with non-syndromic deafnesss, Med. J. Aust. 175 (2001) 191–194.
[32] L.A. Elias, D.D. Wang, A.R. Kriegstein, Gap junction adhesion is necessary for radial migration in the neocortex, Nature 448 (2007) 901–907.
[33] P.E. Martin, G. Blundell, S. Ahmad, R.J. Errington, W.H. Evans, Multiple pathways in the trafficking and assembly of connexin 26, 32 and 43 into gap junction intercellular communication channels, J. Cell Sci. 114 (2001) 3845–3855.
[34] K.A. Schalper, N. Palacios-Prado, M.A. Retamal, K.F. Shoji, A.D. Martínez, J.C. Sáez, Connexin hemichannel composition determines the FGF-1-induced membrane permeability and free $[Ca^{2+}]i$ responses, Mol. Biol. Cell 19 (2008) 3501–3513.

III. 臨床応用の進歩

多能性幹細胞を用いた遺伝性難聴に対する内耳細胞治療法の開発

神谷和作　池田勝久

Inner ear cell therapy for hereditary deafness with multipotent stem cells

Kazusaku Kamiya, Katsuhisa Ikeda
Department of Otorhinolaryngology, Juntendo University School of Medicine

Abstract

Congenital deafness affects about 1 in 1,000 children and the half of them have genetic background such as connexin26 gene mutation. The strategy to rescue such hereditary deafness has not been developed yet. Inner ear cell therapy for hereditary deafness has been studied using some laboratory animals and multipotent stem cells, although the successful reports for the hearing recovery accompanied with supplementation of the normal functional cells followed by tissue repair and recovery of the cellular/molecular functions have been still few. To succeed in hearing recovery by inner ear cell therapy, appropriate cell type, surgical approach and the stem cell homing system to the niche are thought to be required.

Key words: hereditary deafness, mesenchymal stem cell, inner ear, cochlea, connexin26

はじめに

先天性難聴は1,000出生に1人と高頻度に発症し聴覚・言語発育障害の極めて高度なQOLの低下をもたらすが，その半数以上は遺伝性と考えられている．遺伝性難聴の原因遺伝子は代表的なコネキシン26遺伝子(connexin26, Cx26, GJB2)をはじめとして多くが同定されている．しかしその根本的治療法は皆無であり，近年では再生医療の遺伝性難聴への応用が大きく期待されている．著者らは蝸牛線維細胞を標的とした感音性難聴モデルへの内耳細胞治療法に成功し，幹細胞導入により感音性難聴の聴力回復が可能であることを実証した[1]．一方でヒト遺伝性難聴の臨床症状に近いとされる遺伝子改変モデルマウスの開発も進めてきた．ヒト非症候性難聴DFN3モデルBrn4欠損マウス(Brn4KO)は遺伝性難聴の遺伝子改変モデルの先駆けとして報告され，蝸牛線維細胞の変性とそれに伴う内リンパ電位(endocochlear potential: EP)と呼ばれる内耳特異的な電位形成のシステムに異常が生じることが初めて発見された(図1)[2]．更に世界で最も高頻度に変異が検出される代表的な難聴遺伝子，コネキシン26(Cx26)遺伝子(*GJB2*)の優性阻害変異型トランスジェニック(Tg)マウス(Cx26Tg)[3]の作製によっても，高頻度に発生する遺伝性難聴に対する分子病態が明らかになってきた．このマウスは生後発達期に

順天堂大学医学部 耳鼻咽喉科学講座

0047-1852/11/¥60/頁/JCOPY

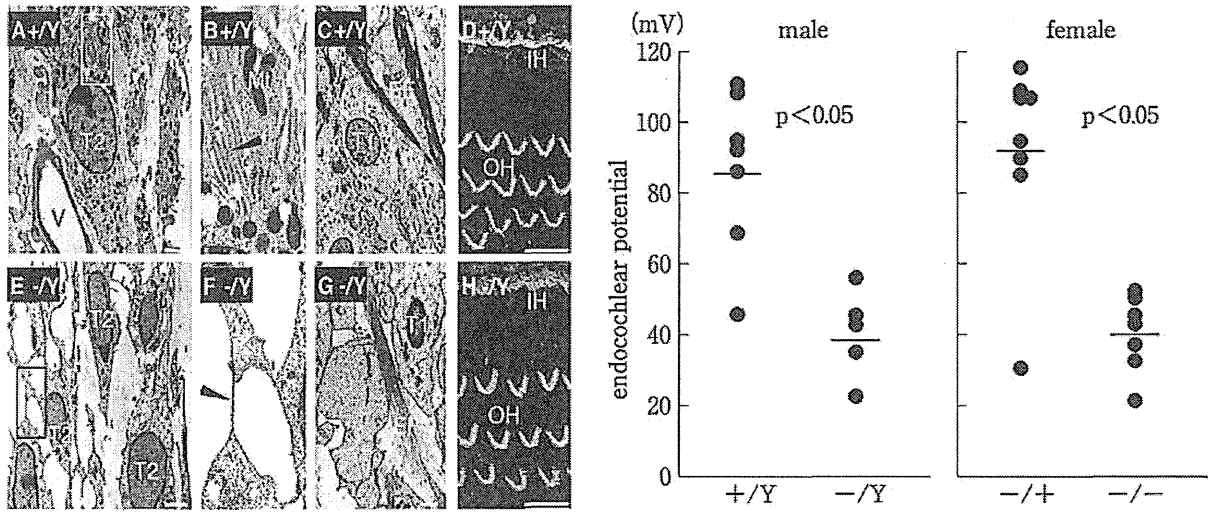

図1　ヒト遺伝性難聴モデルBrn4遺伝子欠損マウスにおける蝸牛線維細胞変性の発見(文献[2]より引用)

蝸牛有毛細胞を含むコルチ器に変性がないにもかかわらず(H)，蝸牛線維細胞に変性がみられ(F，矢頭)，その結果蝸牛内リンパ電位が著しく低下する(右グラフ)．→すなわち蝸牛線維細胞を正常細胞に置換することができれば聴力が回復する可能性が非常に高い．

有毛細胞を含む感覚上皮領域であるコルチ器において，コルチトンネルやヌエル腔などの特殊細胞構築(cytoarchitecture)が正常に形成されないという病理的特徴があるが[4]，外有毛細胞を単離すると正常と同等の有毛細胞特有の運動能を示すことが明らかとなり[5]，残存した有毛細胞を活用した細胞治療により，聴力回復の可能性が十分に考えられる．

著者らの研究チームではCx26の内耳特異的欠損マウス(Cx26cKO)を新規開発し，同モデルマウスによる更なる分子病態の解明とそれに応じた細胞治療法の開発を進めている．

1. 内耳細胞治療の必要性

遺伝性難聴では一部の患者に人工内耳の有用性も報告されているが，本来の聴覚機能を回復させる根本的治療法はいまだ存在しない．遺伝性難聴の第一次的な原因細胞は有毛細胞以外にも蝸牛線維細胞や支持細胞などであることが明らかとなっている．この多様な異常変異細胞を修復するには，新たな治療戦略として多能性幹細胞を用いた効率的細胞治療法の開発が必要であると考えられる．内耳再生医療の技術開発により，これまで補聴器や人工内耳などの適用で根本的治療が存在しなかった遺伝性難聴患者の日常生活における負担は大幅に減り，細胞が永続的に生着すればその後の手術や投薬の頻度が軽減し，極めて現実的な高度医療への発展が期待できる．

2. 内耳への細胞治療とそのアプローチ

近年の内耳再生医療に関する基礎研究分野は，*in vitro*での有毛細胞への分化誘導においては年々進歩している．最近では*in vitro*においてマウス胚性幹(ES)細胞や人工多能性幹(iPS)細胞から聴毛を有する有毛細胞へ分化誘導することも可能となっており[6]，細胞工学的分野では大きな成果が得られている．しかしながらそれらの細胞を移植により内耳組織へ生着させ，同時に機能的補足や組織修復によって聴力回復を誘導する細胞治療の試みは成功例が少なく，引用度の高い論文での報告も少ない．聴力回復を目的とした内耳細胞治療法を開発するためには移植細胞の生着と機能発現を同時に考慮し，内耳の解剖学的特徴および各細胞の生理学的特徴を十分に理解することが重要であると考えられる．

内耳は特殊なリンパ液で満たされた独特な構造をもち，血液-脳関門と同様に‘血液-内耳関

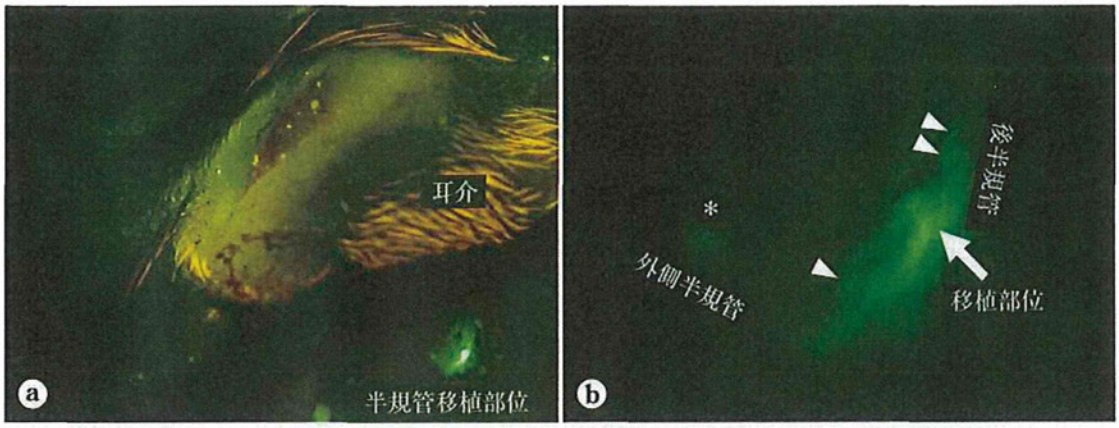

図2 マウスへの間葉系幹細胞移植2週間後の移植部蛍光実体顕微鏡像

a. 耳後部切開により半規管を露出し，移植細胞塊が拒絶されずに生着していることを確認.

b. 更に移植部位より播種性に進展し，コロニーを形成(矢頭). 後半規管から外側半規管への移行も確認された(*).

門'と呼ばれる血管系を有するため内耳有毛細胞やその周辺細胞への薬物的アプローチが難しい. しかし移動能・多分化能を兼ね備えた幹細胞による内耳細胞治療の方法が確立すれば，難聴の根本的治療への有効なツールになると考えられる.

著者らの初期の検討実験では，蝸牛管付近より細胞液投与を試みた際はどの部位でも手術による永続的な聴力低下がみられ，蝸牛組織には線維化が認められた. 著者らはIguchiらの方法[7]を参考にラットの後半規管および外側半規管に小孔を開け[7]，片側から微小チューブを挿入し細胞液の外リンパ腔還流(1×10^5 cells/20 μL×10 min)を行い，良好な結果が得られている. この方法では手術による聴力低下はほとんどみられず，大量の細胞を蝸牛内に導入することができるため，内耳細胞治療に適した投与法であると思われる. 著者らは細胞液環流後に骨髄間葉系幹細胞の細胞塊を半規管の小孔に挿入することにより，内液の漏出を防ぎ，細胞生着にも良好な結果を得ている(図2).

3. *in vitro* での内耳有毛細胞作製法の開発

体外で未分化細胞より内耳有毛細胞を作製しようとする試みは数多く行われてきたが，*in vitro* において有毛細胞特異的マーカーを発現させた報告はこれまで複数報告されてきた. それらを発展させ，遺伝子発現だけではなく特殊な巨大繊毛をもつ内耳有毛細胞に特殊形態を形成させ，最終的には音の振動を感知する機械的刺激受容チャネル(機械電気シグナル変換チャネル：mechanoelectrical transduction(MET) channel)を併せ持つ細胞を作製させる試みがついで行われてきた. 2007年にCorwinらの研究チームはニワトリの間葉系細胞から動毛，不動毛をもつ有毛細胞を作製した[6]. 次段階として，哺乳類細胞から有毛細胞を *in vitro* で作製する技術が期待されてきた. そして2010年，スタンフォード大学のOshima，Hellerらの研究チームによりマウスのES細胞およびiPS細胞から *in vitro* で内耳有毛細胞を作製する画期的技術が発表され，作製された細胞が音の振動を感知できる有毛細胞特有のMET機能を有することが明らかとなった[8]. これにより内耳有毛細胞を体外で人工的に増殖・分化させることが可能であることが示された. この報告では，未分化細胞から内耳前駆細胞へ，段階的に分化を進めているため，これを応用すればすべての内耳構成細胞への分化能をもつ内耳細胞を *in vitro* にて作製し内耳移植に最適な細胞を選抜することが可能となる. 同方法ではES/iPS細胞の浮遊培養後に接着培養を行い分化制御因子としてDkk1，SIS3，IGF-1の添加培養，その後の

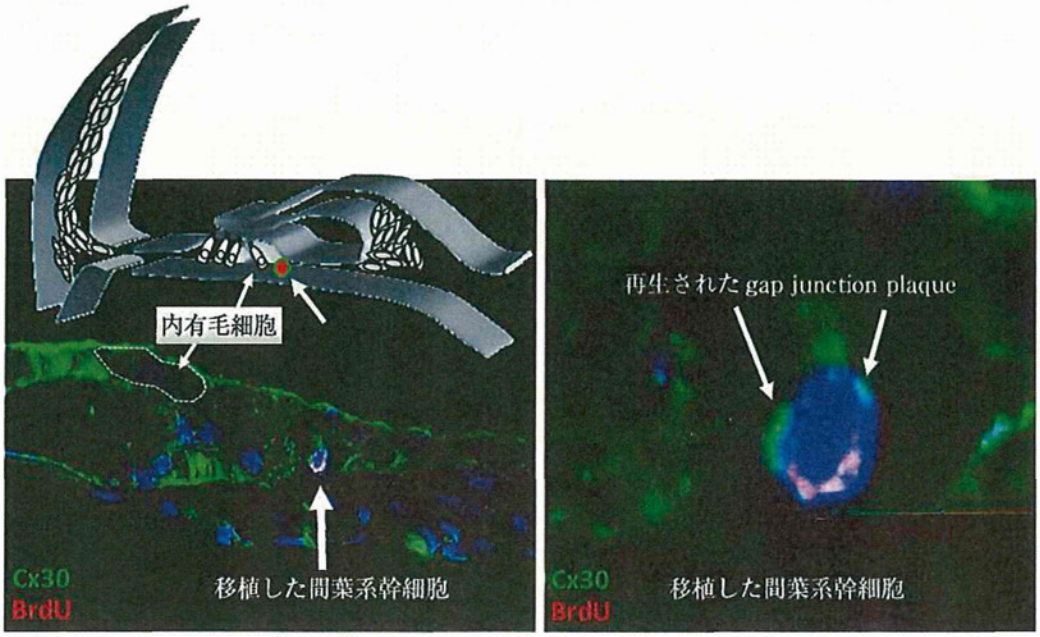

図3　移植した間葉系幹細胞において再生されたギャップ結合プラーク
半規管外リンパ液領域より移植され，コルチ器の内有毛細胞近傍に侵入した間葉系幹細胞(左)．同細胞は蝸牛支持細胞の機能構造であるコネキシン複合体で構成されるギャップ結合プラークを形成している(右)．

bFGF添加後に鶏杯卵形嚢細胞との共培養を行うことで，動毛や機械電気シグナル変換が可能な不動毛をもつ内耳有毛細胞様細胞を得ることを可能としている．

4. 蝸牛標的組織への幹細胞の誘導

前述のように体外で内耳細胞を作製する技術は大きく進展しているが，内耳細胞治療において，作製された細胞を蝸牛組織へ直接的に挿入することは蝸牛の構造上困難であり，適切な箇所に幹細胞を導入できる細胞誘導システムが必須であると考えられる．特に有毛細胞やその支持細胞および内リンパ液に接する血管条細胞，蝸牛線維細胞など，適切な箇所に幹細胞を導入し，その微小環境(niche，ニッチ，ニッシェ)に応じて分化させることが必要である．そのためには適切な幹細胞ホーミング(標的組織へ遊走し微小環境に生着)の分子機構を理解し応用することが重要であると考えられる．

マックスプランク研究所の研究チームは，心筋虚血後に骨髄由来間葉系幹細胞が瘢痕層へ効率的にホーミングされるには走化性因子MCP1とその受容体CCR2およびその下流において細胞遊走を制御しているFROUNTによる分子経路が重要な役割を担っていることを明らかにした[9]．著者らの研究チームでは，実験的に誘発した蝸牛線維細胞損傷部においてもMCP1が高発現することを発見している(文献[1]および未発表データ)．これを応用しCCR2を共発現する骨髄間葉系幹細胞株を作製して内耳細胞治療実験に用いることで，良好な細胞誘導効果が得られている．これまで蝸牛線維細胞領域に軽度損傷を与えた難聴動物では蝸牛線維細胞に移植細胞が侵入しており，一部は有毛細胞の近傍の支持細胞領域に侵入し，同領域の主な機能構造であるギャップ結合プラークを形成した(図3)．

おわりに

将来的に内耳細胞治療への活用が期待できる細胞は，患者の骨髄より樹立可能な骨髄間葉系幹細胞，iPS細胞およびES細胞由来の内耳前駆細胞などであるが，これらの細胞と適切な幹細胞ホーミングの分子機構を応用し適切な遺伝性難聴モデル動物において方法を選抜することに

より，細胞を補うだけではなく遺伝子変異をもつ異常細胞を正常細胞に置換するという全く新しい観点での方法論を確立できる．この方法論の発展により，将来的には多様な遺伝性難聴患者に対し薬物治療などとは異なる，組織損傷の種類と度合いに対応した低リスクで高い効果をもつ新規難聴治療法の開発が期待できる．

文　献

1) Kamiya K, et al: Mesenchymal stem cell transplantation accelerates hearing recovery through the repair of injured cochlear fibrocytes. Am J Pathol **171**: 214-226, 2007.
2) Minowa O, et al: Altered cochlear fibrocytes in a mouse model of DFN3 nonsyndromic deafness. Science **285**: 1408-1411, 1999.
3) Kudo T, et al: Transgenic expression of a dominant-negative connexin26 causes degeneration of the organ of Corti and non-syndromic deafness. Hum Mol Genet **12**: 995-1004, 2003.
4) Inoshita A, et al: Postnatal development of the organ of Corti in dominant-negative Gjb2 transgenic mice. Neuroscience **156**: 1039-1047, 2008.
5) Minekawa A, et al: Cochlear outer hair cells in a dominant-negative connexin26 mutant mouse preserve non-linear capacitance in spite of impaired distortion product otoacoustic emission. Neuroscience **164**: 1312-1319, 2009.
6) Hu Z, Corwin JT: Inner ear hair cells produced in vitro by a mesenchymal-to-epithelial transition. Proc Natl Acad Sci USA **104**: 16675-16680, 2007.
7) Iguchi F, et al: Surgical techniques for cell transplantation into the mouse cochlea. Acta Otolaryngol Suppl (551): 43-47, 2004.
8) Oshima K, et al: Mechanosensitive hair cell-like cells from embryonic and induced pluripotent stem cells. Cell **141**: 704-716, 2010.
9) Belema-Bedada F, et al: Efficient homing of multipotent adult mesenchymal stem cells depends on FROUNT-mediated clustering of CCR2. Cell Stem Cell **2**: 566-575, 2008.

INTERNATIONAL JOURNAL OF Experimental Pathology

Int. J. Exp. Path. (2010)

ORIGINAL ARTICLE

Analysis of subcellular localization of Myo7a, Pcdh15 and Sans in *Ush1c* knockout mice

Denise Yan[1], Kazusaku Kamiya[1], Xiao Mei Ouyang and Xue Zhong Liu

Department of Otolaryngology, University of Miami, Miami, FL, USA

INTERNATIONAL JOURNAL OF EXPERIMENTAL PATHOLOGY

doi: 10.1111/j.1365-2613.2010.00751.x

Received for publication:
30 June 2010
Accepted for publication:
21 October 2010

Correspondence:
Dr Xue Zhong Liu
Department of Otolaryngology (D-48)
University of Miami
1666 NW 12th Avenue
Miami, FL 33136
USA
Tel.: 305 243 5695
Fax: 305 243 4925
E-mail: xliu@med.miami.edu

[1]These authors contributed equally to this work.

Summary

Usher syndrome (USH) is the most frequent cause of combined deaf-blindness in man. An important finding from mouse models and molecular studies is that the USH proteins are integrated into a protein network that regulates inner ear morphogenesis. To understand further the function of harmonin in the pathogenesis of USH1, we have generated a targeted null mutation *Ush1c* mouse model. Here, we examine the effects of null mutation of the *Ush1c* gene on subcellular localization of Myo7a, Pcdh15 and Sans in the inner ear. Morphology and proteins distributions were analysed in cochlear sections and whole mount preparations from $Ush1c^{-/-}$ and $Ush1c^{-/+}$ controls mice. We observed the same distribution of Myo7a throughout the cytoplasm in knockout and control mice. However, we detected Pcdh15 at the base of stereocilia and in the cuticular plate in cochlear hair cells from $Ush1c^{+/-}$ controls, whereas in the knockout $Ush1c^{-/-}$ mice, Pcdh15 staining was concentrated in the apical region of the outer hair cells and no defined staining was detected at the base of stereocilia nor in the cuticular plate. We showed localization of Sans in the stereocilia of controls mouse cochlear hair cells. However, in cochleae from $Ush1c^{-/-}$ mice, strong Sans signals were detected towards the base of stereocilia close to their insertion point into the cuticular plate. Our data indicate that the disassembly of the USH1 network caused by absence of harmonin may have led to the mis-localization of the Protocadherin 15 and Sans proteins in the cochlear hair cells of $Ush1c^{-/-}$ knockout mice.

Keywords
deafness, inner ear, knockout mouse, Usher 1C, Usher syndrome

Introduction

Usher syndrome (USH) is an autosomal recessive disorder characterized by congenital hearing loss and progressive retinal degradation leading to gradual loss of the visual field and blindness.

Three major clinical subtypes (USH type I, USH type II and USH type III) are distinguished on the basis of differences in the severity of the hearing loss, the presence or absence of vestibular dysfunction and the age of onset of retinitis pigmentosa (RP) (Smith *et al.* 1994). In USH type 1, the hearing loss is profound and vestibular function is absent. The onset of progressive RP is before puberty. Usher syndrome type 2 is associated with less severe deafness, normal vestibular function and onset of RP during or after puberty. Usher syndrome type 3 patients also have milder deafness, but, unlike in USH2, the hearing loss is progressive, there is variable impairment of vestibular function and late-onset RP. Each USH subtype is genetically heterogeneous. To date, seven USH1 loci (USH1B-USH1H) have been identified by linkage analyses of USH1 families. Five of the corresponding genes have been cloned: the actin-based motor protein myosin VIIa (*Myo7a*, *USH1B*) (Gibson *et al.* 1995; Weil *et al.* 1995); two cadherin-related proteins, otocadherin or Cadherin 23 (*Cdh23*, *USH1D*) (Bolz *et al.* 2001; Bork *et al.* 2001) and Protocadherin 15 (*Pcdh15*, *USH1F*) (Ahmed *et al.* 2001; Alagramam *et al.* 2001a); and two scaffold proteins, harmonin (*USH1C*) (Verpy *et al.* 2000; Bitner-Glindzicz *et al.* 2000) and Sans (*USH1G*) (Kikkawa *et al.* 2003; Weil *et al.* 2003). The USH proteins are involved in hair bundle morphogenesis in the inner ear by means of protein–protein interactions. In a combination of cell cotransfection

and *in vitro* binding assays, harmonin has been shown to bind to any of the other USH proteins (El-Amraoui & Petit 2005; Yan & Liu 2010; Zheng *et al.* 2010).

A mouse mutant has been reported for each of the known *Ush1* genes; shaker1 (*sh1*) for *Myo7a* (Gibson *et al.* 1995), waltzer (*v*) for *Cdh23* (Di Palma *et al.* 2001; Wilson *et al.* 2001), Ames waltzer (*av*) for *Pcdh15* (Alagramam *et al.* 2001b), deaf circler (*dfcr*) and targeted mouse models for *Ush1c* (Johnson *et al.* 2003; Lentz *et al.* 2007; Lefevre *et al.* 2008; Tian *et al.* 2010) and Jackson shaker (*js*) for *Ush1g* (Kikkawa *et al.* 2003). All of these mice are deaf, exhibit vestibular dysfunction and display similar morphological abnormalities in hair bundle development. In all of these models, the hair cell stereocilia vary irregularly in height and splay out from one another indicating defective lateral interactions. Investigations into the localization of the USH proteins within the developing stereocilia in mice, combined with *in vitro* studies to determine the various interactions between the constituent molecules, have revealed an 'Usher interactome' that is responsible for bundle cohesion. Some of the Ush1 mutant mice (*sh1*, *v*, *av*) exhibited electroretinogram anomalies (Libby & Steel 2001), a defective retinal pigment epithelium has been described in *sh1* mice (Gibbs *et al.* 2003, 2004) and retinal degeneration has been reported in *Ush1c216AA* knockin-in mice (Lentz *et al.* 2010).

The gene encoding harmonin consists of 28 coding exons, alternative splicing of which leads to 10 USH1C isoforms. These alternative transcripts form three subclasses (a, b and c) depending on the domain composition of the protein. The isoform 'a' transcript subclass is expressed ubiquitously in many tissues, whereas the longest 'b' transcript is restricted largely to the inner ear. The short isoform 'c' has a much broader tissue distribution. The harmonin isoforms differ in the number of protein–protein interaction domains (PDZ, postsynaptic density/disc-large/zonal occludens 1), coiled–coiled domains (CC) and the presence of a proline-serine-threonine-rich domain (Verpy *et al.* 2000). Deaf circler, *dfcr* and *dfcr-2J* spontaneous mutant mice have been described as models for human *USH1C*. The mutant *dfcr* is defective in all harmonin isoforms (a, b and c). Only the harmonin b isoform subclass is affected by the *dfcr-2J* mutation (Johnson *et al.* 2003). However, altered harmonin isoforms may retain partial function because the normal reading frame of the *Ush1c* transcripts is not changed in the shortened *dfcr* transcripts of either isoform a or isoform b. Furthermore, none of the three PDZ-encoding domains are deleted in *dfcr* mutant transcripts. Both a USH1C knockin and knockout mouse have also been reported (Lentz *et al.* 2007; Lefevre *et al.* 2008). To further understand the role of harmonin in the pathogenesis that leads to USH1, we have recently generated a targeted null mutation *Ush1c* mouse model in which the first four exons of the *Usher 1c* gene have been replaced by a reporter gene (Liu *et al.* 2005; Yan *et al.* 2006; Tian *et al.* 2010). Our model is unique because none of the previous targeted mouse models for USH1C include a reporter gene in the construct to facilitate expression analysis in various tissues. Here, we examine the effects of *Ush1c* mutation on spatial subcellular localization of Myo7a, Pcdh15 and Sans proteins in the inner ear. In whole mount of inner ears from mutant, Myo7a was not affected at the timepoint we analysed the mutant mice, although it is a critical part of the USH interactome. However, we found both Pcdh15 and Sans displayed an altered localization in the mutant mice that may have resulted from disruption of the entire USH1 complex.

Materials and methods

Inner ears isolated from the $Ush1c^{-/-}$ and$^{+/-}$ mice at postnatal day 21 (PD21) were fixed by immersion in 4% paraformaldehyde (pH 7.4) for 2-5 h at 4°C. The organ of Corti was dissected from the cochlear spiral in phosphate-buffered saline (PBS) using a fine needle. Samples were then permeabilized in 0.5% Triton X-100 for 30 min, then washed in PBS. Non-specific binding sites were blocked using 5% normal goat serum (Life Technologies, Gaithersburg, MD, USA) and 2% bovine serum albumin (ICN, Aurora, OH, USA) in PBS for 2 h. Samples were incubated for 2 h in the primary antibodies at 5 μg/ml in blocking solution. After several rinses in PBS, samples were incubated in Alexa Fluor 488-conjugated anti-rabbit IgG goat at 1:400 (Molecular Probes, Eugene, OR, USA) for 40 min. Samples were mounted using a ProLong Antifade kit (Molecular Probes) and analysed with a laser scanning confocal microscope (LSM-510; Zeiss, Thornwood, NY, USA). The polyclonal antibody against Myo7a (ab3481) was obtained from Abcam (Cambridge, MA, USA). The anti-PCDH15 antibody was generated against a mixed peptide sequence corresponding to amino acid 24-37 (SWGQYDDDWQYEDC) and amino acid 1847-1860 (C+TFTTQPPASNPQWG), and the anti-USH1G antibody was against the central portion of the Sans protein (amino acid 354-372).

Results

Homozygous mutant mice ($Ush1c^{-/-}$) exhibit the abnormal behaviour (circling and/head-tossing) that are typical of mice with profound hearing loss and vestibular dysfunction. $Ush1c^{-/-}$ mice were completely deaf, as there was no detectable auditory-evoked brainstem response (ABR) with 100 dB SPL stimuli, whereas age-matched $Ush1c^{+/-}$ controls showed ABR thresholds in the normal hearing-range at PD15 and PD22. Examination of hair cell surface preparations by scanning electron microscopy from birth (PD0) to PD120 in $Ush1c^{-/-}$ showed progressively disorganized outer hair cell (OHC) stereocilia compared with the well-organized pattern and rigid structure typical of normal stereocilia. Stereocilia of inner hair cells (IHCs) of mutant mice also exhibited a disorganized appearance, but to a lesser degree than did the OHCs (Tian *et al.* 2010).

To address the possibility that absence of harmonin disrupts the USH1 protein complex, we analysed in this study the distribution of Myosin VIIa protein in whole mounts, and of Protocadherin 15 and Sans in cross sections, of inner

ears from *Ush1c*$^{-/-}$ mice. Light microscopy examinations of sections through apical regions of the cochleae of *Ush1c*$^{-/-}$ at PD2 revealed no apparent hair cell degeneration (data not shown). However, in cochlear whole mounts from *Ush1c*$^{-/-}$ mice at PD21, some gaps are seen in the regular array of hair cells. Although the single row of IHCs and the three rows of OHCs can be distinguished by surface scanning of the hair cells (Figure 1b), fragmentation of the OHC stereociliary bundles into two clumps was observed, instead of an integral, single 'V'-shaped bundle as in wild-type hair cells (Figure 1d, arrow). This fragmented aspect was not detected in stereocilia of IHCs at this timepoint (IHC; Figure 1b), suggesting that they were beginning to degenerate. However, confocal microscopic analysis of the hair cells in the basal layer revealed structural morphological abnormalities in both OHCs and IHCs, with a more disorganized appearance in IHC (Figure 1f). Scanning electron microscopy of *Ush1c*$^{-/-}$ mice from PD21 to PD120 showed a progressive degeneration of the hair cells and stereocilia of the cochlea (Tian *et al.* 2010). Myosin 7a has previously been shown to be expressed within the stereocilia and within the cuticular plate, which anchors the base of each stereocilium. In the present study, Myosin 7a was distributed throughout the cytoplasm in *Ush1c*$^{-/-}$ and control mice in the labelled hair cells, revealing structural morphological abnormalities characterized by disorganized, misaligned inner and OHCs (Figure 1e, f).

In cochlear hair cells from heterozygous *Ush1c*$^{+/-}$ control mice, we detected Protocadherin 15 at the base of stereocilia and in the cuticular plate (as shown by the arrow in Figure 2c), whereas in the mutant *Ush1c*$^{-/-}$, Protocadherin 15 immunoreactivity was found accumulated in the apical region of the OHC and no defined staining was detected at the base of stereocilia and little Pcdh15 expression was present at the cuticular plate (Figure 2d). Likewise, in the knockout mice, Sans was undetectable in the stereocilia bundles of cochlear hair cells at PD21 (Figures 3b, d), in contrast to the heterozygous controls (*Ush1c*$^{+/-}$, Figure 3c). Instead, strong Sans staining was observed towards the base of stereocilia close to their insertion point into the cuticular plate with a slight staining of the cytoplasmic region of OHC in cochleae from *Ush1c*$^{-/-}$ mice (Figure 3d). These results suggest a mis-localization of the Pcdh15 and Sans proteins in

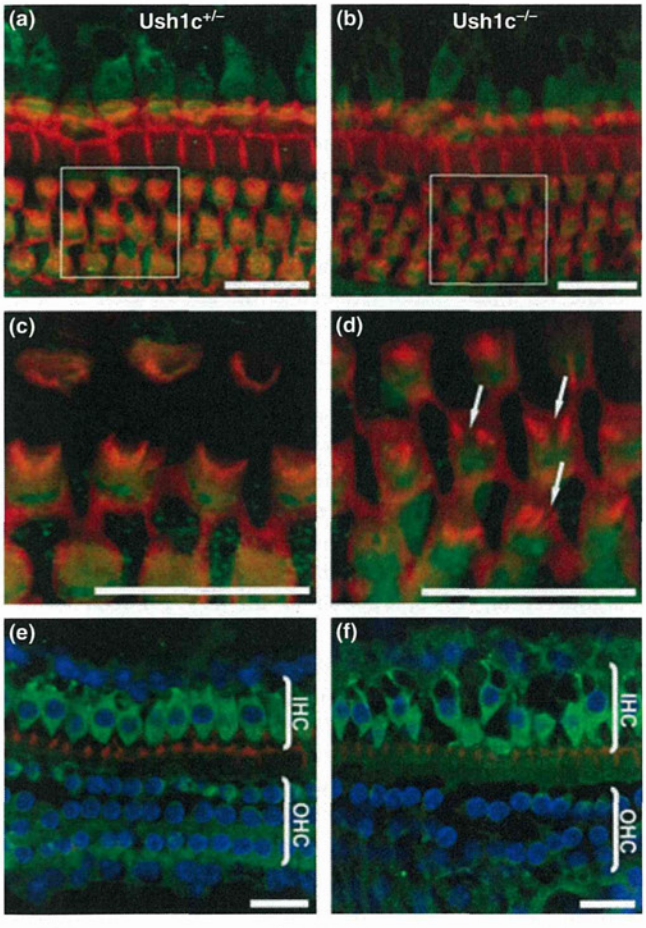

Figure 1 Abnormalities at the apical surface of outer hair cells (OHC) and structural defects of the hair cells in *Ush1c*$^{-/-}$ mice at PD21. Cochlear whole mounts were stained with phalloidin (red) to reveal F-actin in stereocilia and an antibody against myosin 7a (green) to show the basal structure of the hair cells in *Ush1c*$^{+/-}$ (a, c and e) and *Ush1c*$^{-/-}$ mice (b, d and f). Stereocilia defects were observed in the middle part of the stereocilia bundles of the OHCs (d, arrows) that were not detected in stereocilia of inner hair cells (IHC; b). c and d show magnified images corresponding to the boxed areas in a and b respectively. The confocal analysis at the basal level of hair cells with nuclear staining (e and f) (DAPI, Blue). Bars = 20 μm.

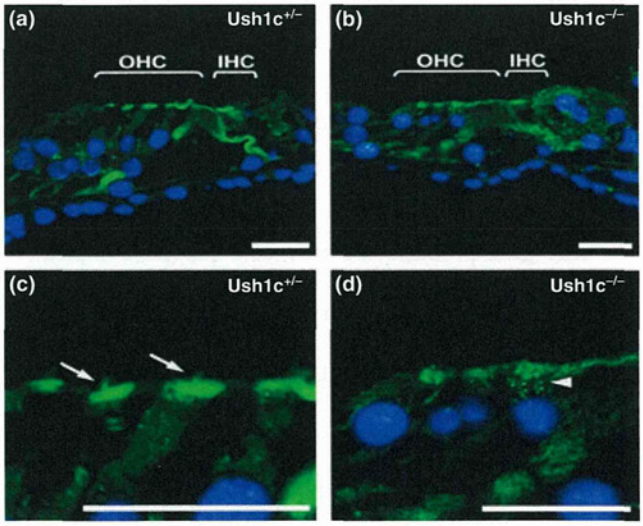

Figure 2 Localization of Protocadherin 15 (green) in the cochlear hair cells of *Ush1c*-knockout mice at PD21. Cross sections of the organ of Corti were stained with an antibody to Protocadherin 15 (green). In *Ush1c*$^{+/-}$ mice (a and c), expression of Protocadherin 15 was localized at the base of stereocilia (left panel, arrow) and in the cuticular plate. In contrast, in *Ush1c*$^{-/-}$ mice (b and d), Protocadherin 15 immunoreactivity appears (arrowhead) diffuse above nuclei (DAPI-Blue). Bars = 20 μm.

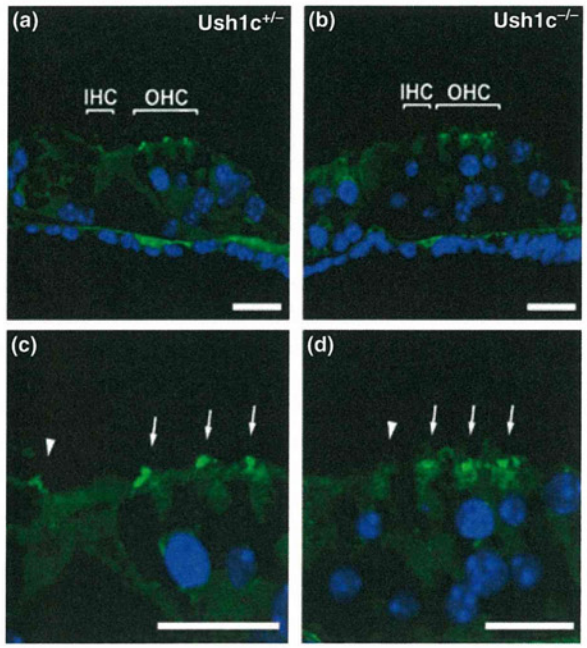

Figure 3 Localization of Sans (green) in the cochlear hair cells of *Ush1c*$^{-/-}$ mice at PD21. Cross sections of the organ of Corti of *Ush1c*$^{+/-}$ (a and c) and *Ush1c*$^{-/-}$ (b and d) mice were stained with an antibody to Sans (green). c and d are higher magnification images of a and b respectively. Arrowheads and arrows indicate inner hair cells and outer hair cells (OHC) respectively. Nuclei were stained by DAPI (Blue). Sans was localized in the stereocilia bundles in *Ush1c*$^{+/-}$ cochlear hair cells at PD21 (c). However, in *Ush1c*$^{-/-}$ mice, strong signals were observed towards the base of stereocilia close to their insertion into the cuticular plate with a slight cytoplasmic staining of OHC (d). Bars indicate 20 μm.

Ush1c$^{-/-}$ mice, characterized by a shift of the immunoreactivity of the proteins towards the base of stereocilia.

Discussion

The USH gene products are part of a protein complex in hair cells of the inner ear. The actin-bundling and PDZ-domain-containing protein harmonin may coordinate the activities of the USH proteins and bridge them to the cytoskeleton of the hair cell (Boeda *et al.* 2002). Disruption of the USH protein network leads to stereociliary disorganization, as observed in mouse models, and is thought to be responsible for congenital deafness in patients with USH (Petit 2001).

Mouse models for USH have played a crucial role in identifying defective genes responsible for USH1 in humans and furthering our understanding of the function of USH1 proteins in normal and disease conditions. All mouse USH1 models are deaf and exhibit vestibular dysfunction. In these mutants, the sensory cells of the cochlea display anomalies in hair bundle development, indicating an essential function for USH1 proteins in stereocilia differentiation (El-Amraoui & Petit 2005). The abnormal stereocilia morphology observed in our *Ush1c* knockout mice is similar to that reported in mouse models for other forms of human USH1.

Regarding spatiotemporal expression, immunohistochemical studies show that the USH1 proteins are expressed in hair cells of the inner ear throughout life. However, USH1 protein subcellular distribution in the stereocilia varies dramatically during development until maturity is reached. Expression of harmonin, Cdh23 and Pcdh15 is detectable in the hair bundle from the moment the bundle emerges at the apical surface of sensory hair cells (Boeda *et al.* 2002; Ahmed *et al.* 2003). Harmonin b is found concentrated at the tips of stereocilia during early postnatal stages but its expression diminishes around PD30 in both the cochlea and vestibule (Boeda *et al.* 2002). The spatiotemporal expression pattern of Cdh23 parallels that of harmonin b, being first observed along the entire length of the emerging stereocilia and then restricted to the tip region.

Notably, Grillet *et al.* (2009) have recently shown that harmonin b is a component of the upper tip-link density, where CDH23 inserts into the stereociliary membrane and is required for normal hair cell mechanoelectrical transduction. In foetal cochlea, Pcdh15 can be detected in supporting cells, outer sulcus cells and the spiral ganglion (Alagramam *et al.* 2001b), while in the mature inner ear, Pcdh15 is also localized in stereocilia of sensory hair cells of both the cochlea and the vestibular organ (Ahmed *et al.* 2003). CDH23 and PCDH15 have been shown to be present in the transient lateral stereocilial and kinocilial links and that the two cadherin proteins interact to form tip-link filaments in sensory hair cells (Sollner *et al.* 2004; Michel *et al.* 2005; Kazmierczak *et al.* 2007). MYO7A is expressed in the mechanosensory hair cells of the vestibular organ and cochlea where it is predominantly localized in the stereocilia, but is also detected within the cuticular plate and the pericuticular necklace region, which is characterized by a dense ring of vesicles (El-Amraoui *et al.* 1996; Hasson *et al.* 1997; Boeda *et al.* 2002).

In this study, we investigated the effect of the *Ush1c* knockout mice on subcellular expression of Myosin 7a, Pcdh15 and Sans in the inner ear. We observed the same distribution of Myosin 7a expression throughout the cytoplasm in knockout and control mice which may indicate that Myosin 7a is expressed earlier than harmonin. This may also suggest that Myosin 7a does not rely on the presence of harmonin isoforms for its cytoplasmic distribution. Whether the cytoplasmic Myosin 7a requires harmonin for hair cells function, however, remains to be examined. We detected Pcdh15 at the base of stereocilia and in the cuticular plate in cochlear hair cells from *Ush1c*$^{+/-}$ controls, whereas in the mutant *Ush1c*$^{-/-}$, Pcdh15 immunoreactivity was found accumulated in the apical region of the OHC and no defined staining was detected at the base of stereocilia nor in the cuticular plate. The scaffold protein Sans has previously been shown localized in the apical hair cell bodies underneath the cuticular plate of cochlear and vestibular hair cells of PD3 mice (Adato *et al.* 2005), but not in the stereocilia. Using an antibody against a peptide sequence corresponding

to the central portion of Sans (amino acid 354–372), we found the protein localized in the stereocilia bundles of mouse cochlear hair cells at PD21 in controls mouse. However, in cochleae from *Ush1c*$^{-/-}$ mice, strong Sans signals were observed towards the base of stereocilia close to their insertion point into the cuticular plate with a slight staining of the cytoplasmic region of OHC. Overall, our data indicated that in mice deficient in harmonin, both interacting partners Pcdh15 and Sans are mislocalized. The epitopes recognized by our antibodies against Pcdh15 and Sans were shifted towards the basal body of the hair cells, whereas they are expressed in the stereocilia of normal control mice.

Acknowledgements

The work is supported by NIH DC05575. We thank Qing Y Zheng for providing *Ush1c* knockout mice DC007392.

References

Adato A., Michel V., Kikkawa Y. *et al.* (2005) Interactions in the network of Usher syndrome type 1 proteins. *Hum. Mol. Genet.* **14**, 347–356.

Ahmed Z.M., Riazuddin S., Bernstein S.L. *et al.* (2001) Mutations of the protocadherin gene pcdh15 cause usher syndrome type 1F. *Am. J. Hum. Genet.* **69**, 25–34.

Ahmed Z.M., Riazuddin S., Riazuddin S., Wilcox E.R. (2003) The molecular genetics of Usher syndrome. *Clin. Genet.* **63**, 431–444.

Alagramam K.N., Yuan H., Kuehn M.H., Murcia C.L., Wayne S., Srisailpathy C.R. (2001a) Mutations in the novel protocadherin pcdh15 cause usher syndrome type 1f. *Hum. Mol. Genet.* **10**, 1709–1718.

Alagramam K.N., Murcia C.L., Kwon H.Y., Pawlowski K.S., Wright C.G., Woychik R.P. (2001b) The mouse ames waltzer hearing-loss mutant is caused by mutation of pcdh15, a novel protocadherin gene. *Nat. Genet.* **27**, 99–102.

Bitner-Glindzicz M., Lindley K.J., Rutland P. *et al.* (2000) A recessive contiguous gene deletion causing infantile hyperinsulinism, enteropathy and deafness identifies the usher type 1c gene. *Nat. Genet.* **26**, 56–60.

Boeda B., El-Amraoui A., Bahloul A. *et al.* (2002) Myosin VIIa, harmonin and cadherin 23, three Usher I gene products that cooperate to shape the sensory hair cell bundle. *EMBO J.* **21**, 6689–6699.

Bolz H., von Brederlow B., Ramírez A. *et al.* (2001) Mutation of CDH23, encoding a new member of the cadherin gene family, causes Usher syndrome type 1D. *Nat. Genet.* **27**, 108–112.

Bork J.M., Peters L.M., Riazuddin S. *et al.* (2001) Usher syndrome 1D and nonsyndromic autosomal recessive deafness DFNB12 are caused by allelic mutations of the novel cadherin-like gene CDH23. *Am. J. Hum. Genet.* **68**, 26–37.

Di Palma F., Holme R.H., Bryda E.C. *et al.* (2001) Mutations in cdh23, encoding a new type of cadherin, cause stereocilia disorganization in waltzer, the mouse model for usher syndrome type 1d. *Nat. Genet.* **27**, 103–107.

El-Amraoui A., Petit C. (2005) Usher I syndrome: unravelling the mechanisms that underlie the cohesion of the growing hair bundle in inner ear sensory cells. *J. Cell Sci.* **118**, 4593–4603.

El-Amraoui A., Sahly I., Picaud S., Sahel J., Abitbol M., Petit C. (1996) Human Usher 1B/mouse shaker-1: the retinal phenotype discrepancy explained by the presence/absence of myosin VIIA in the photoreceptor cells. *Hum. Mol. Genet.* **5**, 1171–1178.

Gibbs D., Kitamoto J., Williams D.S. (2003) Abnormal phagocytosis by retinal pigmented epithelium that lacks myosin VIIa, the Usher syndrome 1B protein. *Proc. Natl Acad. Sci. USA* **100**, 6481–6486.

Gibbs D., Azarian S.M., Lillo C. *et al.* (2004) Role of myosin VIIa and Rab27a in the motility and localization of RPE melanosomes. *J. Cell Sci.* **117**, 6473–6483.

Gibson F., Walsh J., Mburu P. *et al.* (1995) A type VII myosin encoded by the mouse deafness gene shaker-1. *Nature* **374**, 62–64.

Grillet N., Xiong W., Reynolds A. *et al.* (2009) Harmonin mutations cause mechanotransduction defects in cochlear hair cells. *Neuron* **62**, 375–387.

Hasson T., Gillespie P.G., Garcia J.A. *et al.* (1997) Unconventional myosins in inner-ear sensory epithelia. *J. Cell Biol.* **137**, 1287–1307.

Johnson K.R., Gagnon L.H., Webb L.S. *et al.* (2003) Mouse models of ush1c and dfnb18: phenotypic and molecular analyses of two new spontaneous mutations of the ush1c gene. *Hum. Mol. Genet.* **12**, 3075–3086.

Kazmierczak P., Sakaguchi H., Tokita J. *et al.* (2007) Cadherin 23 and protocadherin 15 interact to form tip-link filaments in sensory hair cells. *Nature* **6**, 449.

Kikkawa Y., Shitara H., Wakana S. *et al.* (2003) Mutations in a new scaffold protein sans cause deafness in jackson shaker mice. *Hum. Mol. Genet.* **12**, 453–461.

Lefevre G., Michel V., Weil D. *et al.* (2008) A core cochlear phenotype in ush1 mouse mutants implicates fibrous links of the hair bundle in its cohesion, orientation and differential growth. *Development* **135**, 1427–1437.

Lentz J., Pan F., Ng S.S., Deininger P., Keats B.J. (2007) Ush1c216a knock-in mouse survives katrina. *Mutat. Res.* **616**, 139–144.

Lentz J.J., Gordon W.C., Farris H.E. *et al.* (2010) Deafness and retinal degeneration in a novel USH1C knock-in mouse model. *Dev. Neurobiol.* **70**, 253–267.

Libby R.T., Steel K.P. (2001) Electroretinographic anomalies in mice with mutations in Myo7a, the gene involved in human Usher syndrome type 1B. *Invest. Ophthalmol. Vis. Sci.* **42**, 770–778.

Liu X.Z., Zheng Q.Y., Ouyang X.M., Du L.L., Johnson K.R., Yan D. (2005) Gene targeting and homologous recombination for USH1C gene. *Association for Research in Otolaryngology Meeting*. New Orleans, LA: The Fairmont February, 19–24.

Michel V., Goodyear R.J., Weil D. *et al.* (2005) Cadherin 23 is a component of the transient lateral links in the developing hair bundles of cochlear sensory cells. *Dev. Biol.* **280**, 281–294.

Petit C. (2001) Usher syndrome: from genetics to pathogenesis. *Annu. Rev. Genomics Hum. Genet.* **2**, 271–297.

Smith R.J., Berlin C.I., Hejtmancik J.F. *et al.* (1994) Clinical diagnosis of the Usher syndromes. Usher Syndrome Consortium. *Am. J. Med. Genet.* **50**, 32–38.

Sollner C., Rauch G.J., Siemens J. *et al.* (2004) Mutations in cadherin 23 affect tip links in zebrafish sensory hair cells. *Nature* **428**, 955–959.

Tian C., Liu X.Z., Han F. *et al.* (2010) Ush1c gene expression levels in the ear and eye suggest different roles for Ush1c in neurosensory organs in a new Ush1c knockout mouse. *Brain Res.* **1328**, 57–70.

Verpy E., Leibovici M., Zwaenepoel I. *et al.* (2000) A defect in harmonin, a PDZ domain-containing protein expressed in the inner ear sensory hair cells, underlies usher syndrome type 1C. *Nat. Genet.* **26**, 51–55.

Weil D., Blanchard S., Kaplan J. *et al.* (1995) Defective myosin viia gene responsible for usher syndrome type 1b. *Nature* **374**, 60–61.

Weil D., El-Amraoui A., Masmoudi S. *et al.* (2003) Usher syndrome type 1G (USH1G) is caused by mutations in the gene encoding sans, a protein that associates with the ush1c protein, harmonin. *Hum. Mol. Genet.* **12**, 463–471.

Wilson S.M., Householder D.B., Coppola V. *et al.* (2001) Mutations in cdh23 cause nonsyndromic hearing loss in waltzer mice. *Genomics* **74**, 228–233.

Yan D., Liu X.Z. (2010) Genetics and pathological mechanisms of Usher syndrome. *J. Hum.Genet.* **55**, 327–335.

Yan D., Zheng Q.Y., Ouyang X.M. *et al.* (2006) A gene knockout mouse model for Usher syndrome type 1C. *Association for Research in Otolaryngology Meeting*. Baltimore, February 2006.

Zheng L., Zheng J., Whitlon D.S., García-Añoveros J., Bartles J.R. (2010) Targeting of the hair cell proteins cadherin 23, harmonin, myosin XVa, espin, and prestin in an epithelial cell model. *J. Neurosci.* **30**, 7187–7201.

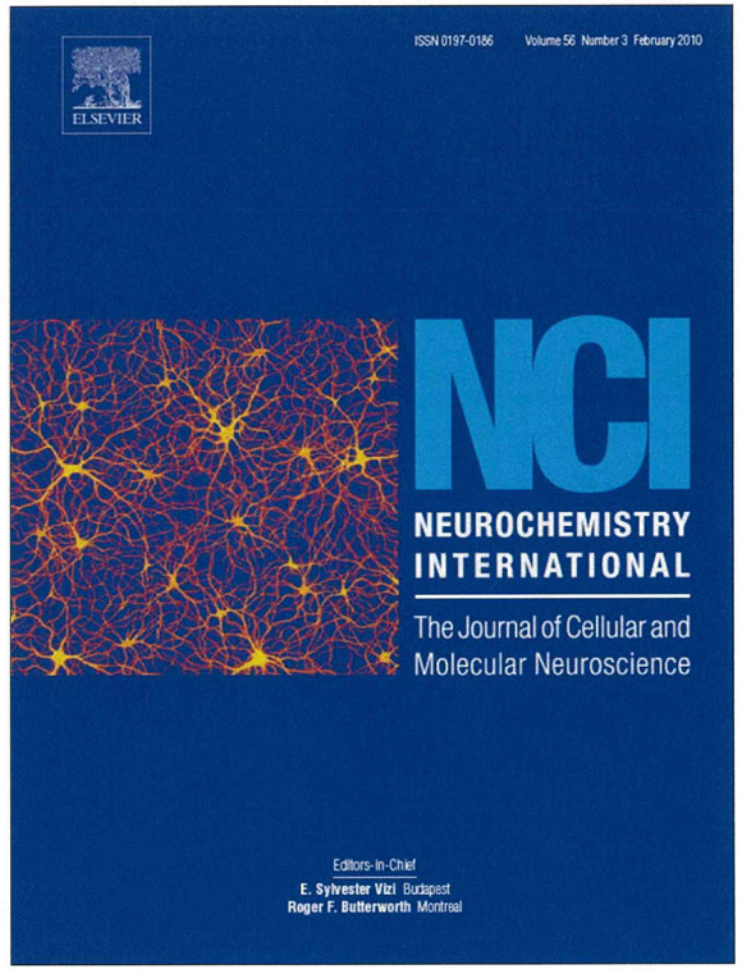

Neurochemistry International 56 (2010) 487–494

Contents lists available at ScienceDirect

Neurochemistry International

journal homepage: www.elsevier.com/locate/neuint

Enhanced expression of C/EBP homologous protein (CHOP) precedes degeneration of fibrocytes in the lateral wall after acute cochlear mitochondrial dysfunction induced by 3-nitropropionic acid

Yoshiaki Fujinami [a], Hideki Mutai [a], Kazusaku Kamiya [a], Kunio Mizutari [a], Masato Fujii [b], Tatsuo Matsunaga [a,*]

[a] Laboratory of Auditory Disorders, National Institute of Sensory Organs, National Tokyo Medical Center, 2-5-1 Higashigaoka, Meguro-ku, Tokyo 152-8902, Japan
[b] Division of Hearing and Balance Research, National Institute of Sensory Organs, National Tokyo Medical Center, Meguro-ku, Tokyo 152-8902, Japan

ARTICLE INFO

Article history:
Received 28 September 2009
Received in revised form 28 November 2009
Accepted 14 December 2009
Available online 21 December 2009

Keywords:
Cochlea
Mitochondria
Apoptosis
Endoplasmic reticulum stress
Oxidative stress

ABSTRACT

We previously reported that treatment of the rat cochlea with a mitochondrial toxin, 3-nitropropionic acid (3-NP), causes temporary to permanent hearing loss depending on the amount of the drug. Furthermore, apoptosis of cochlear lateral wall fibrocytes, which are important for maintaining the endolymph, is a predominant pathological feature in this animal model. 3-NP is known to induce oxidative stress as well as neuronal apoptosis. C/EBP homologous protein gene (*chop*) is one of the marker genes induced during endoplasmic reticulum (ER) stress, and is also considered to be involved in apoptosis. To elucidate the molecular mechanism of cochlear fibrocyte apoptosis induced by 3-NP, we studied spatiotemporal expression of C/EBP homologous protein (CHOP) and other signaling molecules related to ER stress as well as the appearance of apoptotic cells in the cochlear lateral wall after 3-NP treatment. Quantitative real-time PCR revealed that *chop* and activating transcription factor 4 gene (*atf-4*) showed marked increase within 6 h, whereas expression of other ER stress-responsive genes such as *grp78* and *grp94* did not change. Immunohistochemistry showed that 3-NP treatment caused up-regulation of CHOP, especially in type II and type IV fibrocytes, followed by the appearance of terminal deoxynucleotidyl transferase mediated dUTP nick end-labeling (TUNEL)-positive apoptotic cells in the same confined area. Thus, apoptosis of lateral wall fibrocytes induced by 3-NP is likely to be mediated by induction of CHOP. These results contribute clarification of pathological mechanism of cochlear fibrocytes and may lead to development of novel therapeutic strategy for hearing loss.

1. Introduction

Recent advances in auditory research have helped build strategies to cure hearing loss by sensory cell regeneration or prevention of sensory cell loss (Holley, 2005; Kelley, 2006). Most experimental animal models of auditory disorders indicate that noise-induced, hereditary, and drug-induced hearing loss is caused by degeneration of the sensory hair cells or spiral ganglion cells. Recently, several studies reported the involvement of fibrocytes degeneration in the cochlear lateral wall (LW) in hereditary hearing loss (Minowa et al., 1999; Delprat et al., 2005), age-related hearing loss (Spicer and Schulte, 2002), and noise-induced hearing loss (Wang et al., 2002), implying that these non-sensory cells also play important roles in hearing.

We recently established an animal model of acute hearing loss, which is primarily caused by degeneration of LW fibrocytes, using the mitochondrial toxin 3-nitropropionic acid (3-NP) (Hoya et al., 2004; Okamoto et al., 2005; Kamiya et al., 2007; Mizutari et al., 2008). In this model, only less than a 2-fold difference in 3-NP dose differentiates between temporary and irreversible hearing loss. Appearance of TUNEL positive cells (Kamiya et al., 2007; Mizutari et al., 2008), and blockade of fibrocyte degeneration by caspase inhibitor (Mizutari et al., 2008) indicate that degeneration of LW fibrocytes is mainly apoptosis in this model. LW fibrocytes are critical for maintaining the ion concentration of the endolymph by K^+ recycling from the perilymph (Schulte and Steel, 1994; Spicer and Schulte, 1998); and disturbance of the endolymphatic ion concentration leads to immediate hearing loss. Fibrocytes of the LW are divided into five cell types based on structural features, immunostaining patterns and general location (Schulte and Adams, 1989; Spicer and Schulte, 1996; Mutai et al., 2009). Type II and type IV fibrocytes contain numerous mitochondria, and endoplasmic

* Corresponding author. Tel.: +81 3 3411 0111; fax: +81 3 3411 0185.
E-mail address: matsunagatatsuo@kankakuki.go.jp (T. Matsunaga).

0197-0186/$ – see front matter © 2009 Elsevier Ltd. All rights reserved.
doi:10.1016/j.neuint.2009.12.008

reticulum (ER) expresses various types of ion transporters, channels, and pumps, and have significant roles in maintenance of the endolymph. 3-NP is considered to elicit acute deafness by depleting energy in the cochlea, which primarily induces apoptosis of type II and type IV fibrocytes followed by perturbation of endolymph homeostasis. Understanding the molecular pathway of LW fibrocytes cell death is likely to provide insight for preventing auditory disorders caused by LW fibrocyte dysfunction.

3-NP administration alters gene expression in various tissues and induces apoptosis in neuronal cells (Behrens et al., 1995; Pang and Geddes, 1997; Sato et al., 1997). C/EBP homologous protein (CHOP) is a DNA binding protein targeted by activating transcription factor 4 (ATF-4). *chop* (encoding CHOP) is one of the marker genes induced in ER stress (Oyadomari and Mori, 2004), which was originally defined as a cellular response against accumulation of unfolded proteins in the ER (Xu et al., 2005). In addition, the accumulation of unfolded proteins in mitochondria also induces CHOP expression (Zhao et al., 2002). CHOP is considered to be involved in apoptosis in various cell types (Matsumoto et al., 1996; Maytin et al., 2001). Part of the downstream pathways of CHOP that leads to apoptosis was recently revealed. It was reported that overexpression of Bcl-2 blocks CHOP-induced apoptosis (Matsumoto et al., 1996), Tribbles-related protein 3 (TRB3) repress the transcriptional activity of CHOP (Ohoka et al., 2005) and Bcl-2 interacting mediator of cell death (Bim) is closely related to the CHOP-induced apoptosis (Puthalakath et al., 2007). CHOP expression is induced in Parkinson's disease (Holtz and O'Malley, 2003), ischemia–reperfusion injury (Tajiri et al., 2004), and diabetes (Araki et al., 2003). The linkage between CHOP induction and cell death raises the possibility that CHOP may also play a role in eliciting apoptosis of LW fibrocytes exposed to 3-NP. To explore this possibility, we examined the induction of CHOP and other ER stress-related molecules such as *atf-4* gene (encoding an ATF-4) in the LW of 3-NP-treated animals, and the relationship of CHOP expression and apoptosis in the degenerating cells.

2. Results

2.1. Time course of hearing after 3-NP treatment

The time course of hearing in rats treated with 3-NP was measured by auditory brainstem response (ABR). Because our previous studies using the same animal model as the present study showed a remarkable difference in the time course of ABR thresholds at 8 kHz and 20 kHz between TTS and PTS rats, we measured ABR thresholds at these two frequencies in the present study. The rats treated with 300 mM 3-NP demonstrated severe hearing loss at both 8 kHz and 20 kHz (72.0 ± 5.9 dB and 85.5 ± 1.5 dB, respectively) 1 day after the treatment (DAT, Fig. 1). At 7 DAT, the threshold shift at 8 kHz recovered to almost the normal range (15.0 ± 1.2 dB) and the threshold shift at 20 kHz gradually recovered to a moderate level of hearing loss (40.0 ± 8.9 dB). These rats were referred as temporary threshold shift (TTS) rats. In contrast, the ABR threshold in rats treated with 500 mM 3-NP exceeded the highest measurable level at both tested frequencies 3 h after the treatment and did not show any signs of recovery even at 7 DAT. These rats were referred as permanent threshold shift (PTS) rats. Saline-treated rats maintained normal thresholds, indicating that the surgical procedures did not cause hearing loss. These phenotypes were consistent with our previous data (Hoya et al., 2004).

2.2. Time course of chop and atf-4 expression in the LW after 3-NP treatment

To explore the molecular events during hearing loss by 3-NP, we investigated whether the genes activated during ER stress were

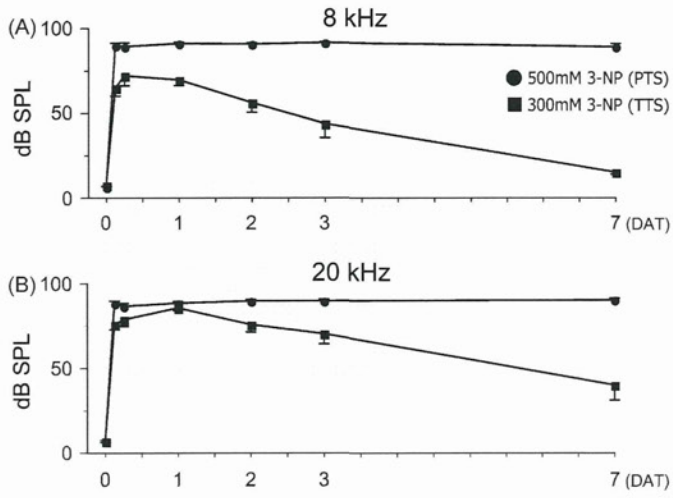

Fig. 1. Time course of auditory thresholds in temporary threshold shift (TTS) rats treated with 300 mM 3-nitropropionic acid (3-NP) and permanent threshold shift (PTS) rats treated with 500 mM 3-NP. The threshold shifts were recorded at 8 kHz (A) and 20 kHz (B). Although the thresholds reached their peak at 1 day after 3-NP treatment (DAT) and then decreased in the TTS rats, the thresholds in the PTS rats exceeded the measurable levels at 3 h after the treatment and were stable at 7 DAT. $n = 5$.

up-regulated in the LW after 3-NP treatment. Expression of four ER stress-responsive genes (*chop*, *atf-4*, *grp78*, and *grp94*) along with the housekeeping gene glyceraldehyde-3-phosphate dehydrogenase (*gapdh*) in the cochlear middle turn of TTS and PTS rats was measured using semi-quantitative reverse transcription PCR (RT-PCR). LW of cochlear middle turn was chosen because histological changes indicating degeneration of LW fibrocytes were evidently detected at this region in both TTS and PTS rats and there was a remarkable difference in the time course of ABR thresholds at this region between TTS and PTS rats.

We found that all five transcripts were successfully amplified in the LW from untreated rats (Fig. 2A). In addition, two of them, *chop* and its activator *atf-4*, both of which are suggested to be involved in activation of the apoptotic pathway, were up-regulated after 3-NP treatment. The changes in *chop* and *atf-4* expression from 3 h to 7 DAT were similar in the TTS and PTS rats; an increase of the PCR bands occurred in TTS and PTS rats within a few hours after treatment, but these band intensities dropped to the untreated levels in TTS rats and even lower in PTS rats at 1 DAT. In contrast, expression of *grp78* and *grp94*, molecular chaperones in the ER lumen and indicators of cell survival (Kaufman, 1999), did not show apparent changes throughout the experimental period (Fig. 2A), indicating that not all the genes mediating ER stress are stimulated in the LW after 3-NP treatment.

In the next experiment, expression levels of *chop* and *atf-4* after 3-NP treatment from which the changes were seen in the RT-PCR results were further evaluated by quantitative real-time RT-PCR (qPCR). These gene expressions were compared with those in untreated rats (0 DAT, $n = 5$). Because neither *grp78* nor *grp94* expression did not change in the screening by RT-PCR, these gene expressions were not measured by qPCR. The level of *chop* (Fig. 2B) was increased at 6 h after the treatment (390 ± 91% in TTS rats, $p < 0.05$, and 595 ± 262% in PTS rats), confirming our previous observation that *chop* is induced promptly after 3-NP treatment. However, no significant difference in the peak level of *chop* was observed between PTS and TTS rats. At 1 DAT, the *chop* level dropped sharply to 53 ± 6% in TTS rats and 58 ± 16% in PTS rats, followed by gradual recovery to the untreated level in TTS and PTS rats until 7 DAT. As observed for *chop*, *atf-4* expression significantly increased and reached its peak 6 h after 3-NP treatment (Fig. 2C). The increase in *atf-4* expression was lower than that in *chop* both in TTS rats

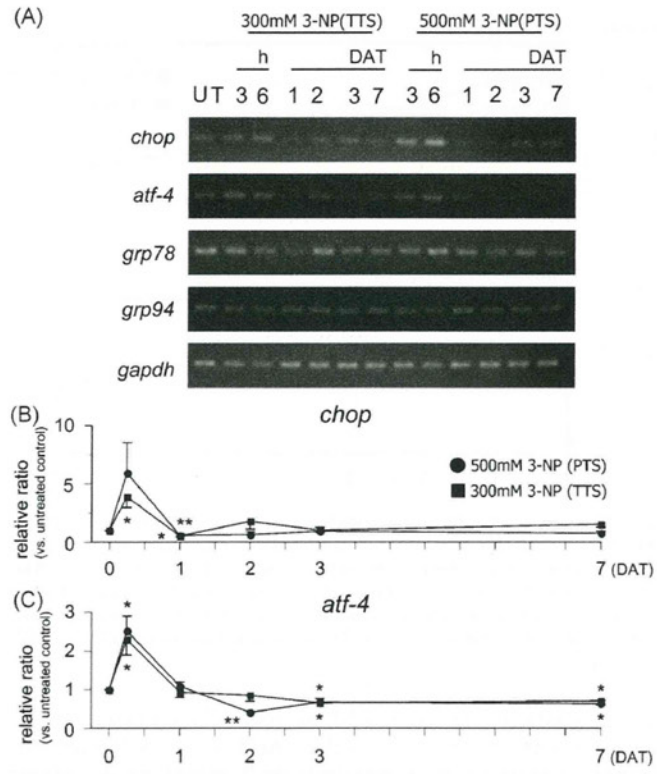

Fig. 2. Expression of ER stress-responsive genes in the lateral wall (LW) after 3-NP treatment. Expression was determined by semi-quantitative reverse transcription PCR (A) and quantitative real-time PCR (B and C). UT; untreated control rats; *gapdh*; glyceraldehyde-3-phosphate dehydrogenase. DAT; day(s) after 3-NP treatment. *chop* (B) and *atf-4* (C) were temporarily induced in the LW 6 h after treatment in both TTS rats treated with 300 mM 3-NP and PTS rats treated with 500 mM 3-NP. *chop* was decreased to approximately half of the untreated level (0 h) at 1 DAT and then recovered to the normal level. $n = 5$. $^{*}p < 0.05$, $^{**}p < 0.01$, significant difference vs. untreated control.

(230 ± 40%, $p < 0.05$) and in PTS rats (252 ± 38%, $p < 0.05$). In the TTS and PTS rats, *atf-4* was down-regulated to 71 ± 10% and 64 ± 8% of the untreated level, respectively, at 7 DAT. Taken together, *chop* and *atf-4*, which are activated by various stimuli including ER stress, were responsive to 3-NP in the present study, whereas expression of the other candidate genes, *grp78* and *grp94*, did not change in response to the treatment.

2.3. Spatial expression patterns of CHOP and apoptosis in the LW after 3-NP treatment

We next investigated spatial expression patterns of the CHOP in the LW after 3-NP treatment. CHOP signals were detected using immunohistochemistry with paraformaldehyde-fixed, paraffin-embedded tissues. We focused on the cochlear middle turn to compare with expression levels of *chop* and *atf-4* by RT-PCR and qPCR. The same primary antibody for CHOP was used in this study as that used for a previous report (Hayashi et al., 2005). To ascertain specific binding of the primary antibody, a set of sections was stained in a similar way without the primary antibody, and the staining was not detected (data not shown). Types of LW fibrocytes were judged based on their localization within the spiral ligament according to the previous studies (Schulte and Adams, 1989; Spicer and Schulte, 1996; Mutai et al., 2009). Fig. 3 shows distribution of the CHOP signal at the middle turn of the LW before and after 3-NP treatment. CHOP was detected at low levels in the LW of untreated and saline-treated rats (Fig. 3A and F). The low CHOP signal level persisted until 6 h after treatment in both TTS and PTS rats (Fig. 3B and G). The CHOP signal intensity started to increase over the entire spiral ligament at 1 DAT in both TTS and PTS rats (Fig. 3C and H), with the most intense staining in the area of type II and type IV fibrocytes in PTS rats. At this time in the TTS, CHOP immunoreactivity was localized mainly in the cytoplasm (Fig. 3C and L), and localized slightly also in the nuclei. CHOP immunoreactivity did not remain in the LW at 2 DAT (Fig. 3D). On the other hand, immunoreactivity in the PTS rats at 1 DAT was localized mainly in the nuclei (Fig. 3H and N), and remained in the LW at 2DAT and 3 DAT (Fig. 3I and J). Fibrocyte degeneration was not apparent in the spiral ligament of either TTS or PTS rats until 1 DAT. In TTS rats, fibrocyte degeneration which was indicated by a region free of cellular nuclei was observed in the area of type II and type IV fibrocytes at 2 DAT (Fig. 3D and M) and 3 DAT (Fig. 3E) and area of fibrocyte degeneration did not expand from 2 DAT to 3 DAT. In PTS rats, a subpopulation of type II and type IV fibrocytes started to disappear and CHOP immunoreactivity was detected around this area at 2 DAT (Fig. 3I and O), and a majority of the fibrocytes in the LW had degenerated at 3 DAT (Fig. 3J).

Because our previous study showed that death of LW fibrocytes is mediated by an apoptotic pathway (Kamiya et al., 2007; Mizutari et al., 2008), we next investigated whether the onset of apoptotic cell death coincides with the onset of CHOP induction. The paraffin sections were used for the terminal deoxynucleotidyl transferase mediated dUTP nick end-labeling (TUNEL) assay, a method generally accepted to detect DNA fragmentation caused by activation of apoptotic pathways (Fig. 4). TUNEL-positive cells were not detected in untreated and saline-treated LWs (Fig. 4A and F). In TTS rats (Fig. 4B–E), TUNEL-positive cells appeared at 2 DAT in the area of type II fibrocytes (Fig. 4D and M). A small number of TUNEL-positive cells were also evident at 3 DAT (Fig. 4E). In PTS rats (Fig. 4G–J), TUNEL-positive cells were detectable as early as 1 DAT in the type II/IV fibrocytes (Fig. 4H). The number of TUNEL-positive cells in the LW gradually increased from 1 to 3 DAT (Fig. 4H–J). To clarify whether CHOP induction and apoptotic cell death are associated, the LWs in the untreated or PTS rats were subjected to a double immunofluorescence study (Fig. 5A–J). CHOP signal (red) was low in untreated rats (Fig. 5A, D, E) and intensified in the area of type II and type IV fibrocytes at 1 DAT in PTS rats (Fig. 5F, I, and J). TUNEL-positive apoptotic cells (green) were undetectable in the LW of untreated rats (Fig. 5B, D, and E) but were observed in PTS rats at 1 DAT (Fig. 5G, I, and J). Although apoptotic cells were not convincingly co-immunostained with CHOP in PTS rats at 1 DAT, they were confined to the CHOP-positive area (Fig. 5I and J). In untreated rats, the CHOP signal visualized by fluorescein staining in the stria vascularis (Fig. 5A) was inconsistent with the absence of a signal in the stria vascularis by 3,3′-diaminobenzidine (DAB) staining (Fig. 3A). The difference was considered to be due to the methods used for antigen retrieval. Because apoptotic cells were not detected in the stria vascularis, we focused on the CHOP expression in the spiral ligament. Thus, CHOP expression in the stria vascularis is not discussed further in this study. Overall, we demonstrated that induction of the CHOP signal was followed by apoptotic cell death in the LW fibrocytes after 3-NP treatment.

3. Discussion

In this study, we examined the time course of CHOP expression, apoptosis, and degeneration of fibrocytes after administration of 3-NP. We demonstrated temporary CHOP expression in the confined area of LW in which fibrocyte degeneration occurred afterwards. In TTS rats, TUNEL-positive cells became detectable at 2 DAT, approximately 1 day after CHOP induction. In PTS rats, a few TUNEL-positive cells were detectable at 1 DAT, when the CHOP level was first up-regulated. Then, the number of TUNEL-positive cells increased significantly at 2 DAT. CHOP and TUNEL signals are detectable in the same area, but co-localization of these two

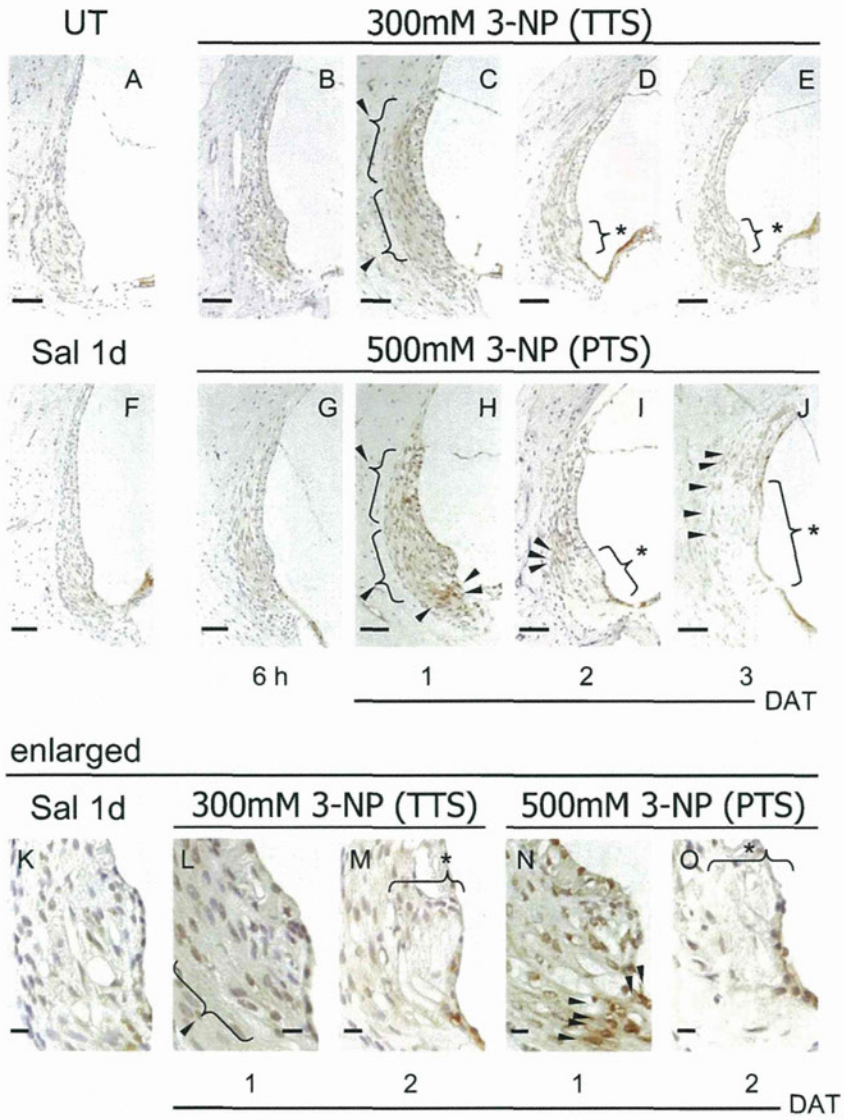

Fig. 3. Immunohistochemical analysis of CHOP expression in the LW after 3-NP treatment. In untreated control rats (UT), a low level of CHOP was detectable in the entire LW (A). In TTS rats treated with 300 mM 3-NP (B–E, L, and M), the CHOP signal (arrowheads) was unchanged at 6 h but intensified 1 day after 3-NP treatment (DAT) (C) compared with saline-treated rats (Sal 1d, F, K). A limited area (asterisk) of the LW had degenerated at 2 DAT and 3 DAT (D, E). In PTS rats treated with 500 mM 3-NP (G–J, N, and O), an intense CHOP signal (arrowheads) was evident, especially in the area of type II and type IV fibrocytes of the LW at 1 DAT (H). At 2 DAT, type II and type IV fibrocytes appeared to start degeneration (asterisk) (I), and the area of degenerated fibrocytes expanded at 3 DAT (J). K–O are enlarged images of spiral prominence of F, C, D, H and I, respectively. Scale bar ≈ 50 μm (A–J) and 10 μm (K–O).

staining was not detected. Because CHOP is known to be involved in inducing apoptosis (Matsumoto et al., 1996; Maytin et al., 2001), we speculate that the delay of TUNEL appearance is due to signal transduction for apoptotic pathways. Tajiri et al. (2004) reported that *chop* induction in the striatum peaks 12 h after the occlusion of the carotid artery, followed by detection of numerous TUNEL-positive cells at 24 h. Investigation of signaling molecules downstream of CHOP (Wang et al., 1998; Sok et al., 1999) and activation of pro-apoptotic molecules such as caspases after 3-NP treatment may clarify the direct association of CHOP activation with apoptotic cell death in LW fibrocytes. In the present study, of note is that nuclei were also positively stained for CHOP in PTS rats at 1 DAT, which is required to exert functional effect for this transcription factor (Zinszner et al., 1998).

The activation of ATF-4 and CHOP in the LW of 3-NP-treated rats is reminiscent of CHOP and ATF-4 activation in ischemic brain (Hayashi et al., 2005). Induction of the same molecules in these two affected areas is probably caused by the features of energy depletion which are shared by mitochondrial dysfunction and ischemia. What is the mechanism of the expression of *atf-4* and CHOP which is the downstream target of ATF-4 in LW fibrocytes? The mitochondrial toxin 3-NP is an irreversible inhibitor of succinate dehydrogenase (complex II of the electron transport chain) (Coles et al., 1979). Inhibition of energy metabolism by 3-NP results in the production of reactive oxygen species (Beal et al., 1995; Lee et al., 2002; Rosenstock et al., 2004) that causes oxidative stress and neuronal cell death (Behrens et al., 1995; Pang and Geddes, 1997; Sato et al., 1997; Higuchi, 2004). Oxidative stress induces ER stress (Yu et al., 1999), and this is known to enhance CHOP expression (Oyadomari and Mori, 2004). In addition, cells exposed to 3-NP also release mitochondrial Ca^{2+}, which is caused by an increasing amount of reactive oxygen species (Rosenstock et al., 2004) and rapid elevation of the intracellular Ca^{2+} level is known to enhance CHOP expression (Deshpande et al., 1997; Tanaka et al., 2005). Thus, oxidative stress, ER stress and increase in the intracellular Ca^{2+} level are related events in terms of the molecular signaling pathways. We assume 3-NP induced ATF-4 and CHOP in LW by these mechanism.

Our findings are not in full agreement with the hypothesis that CHOP is activated exclusively in response to ER stress in the LW

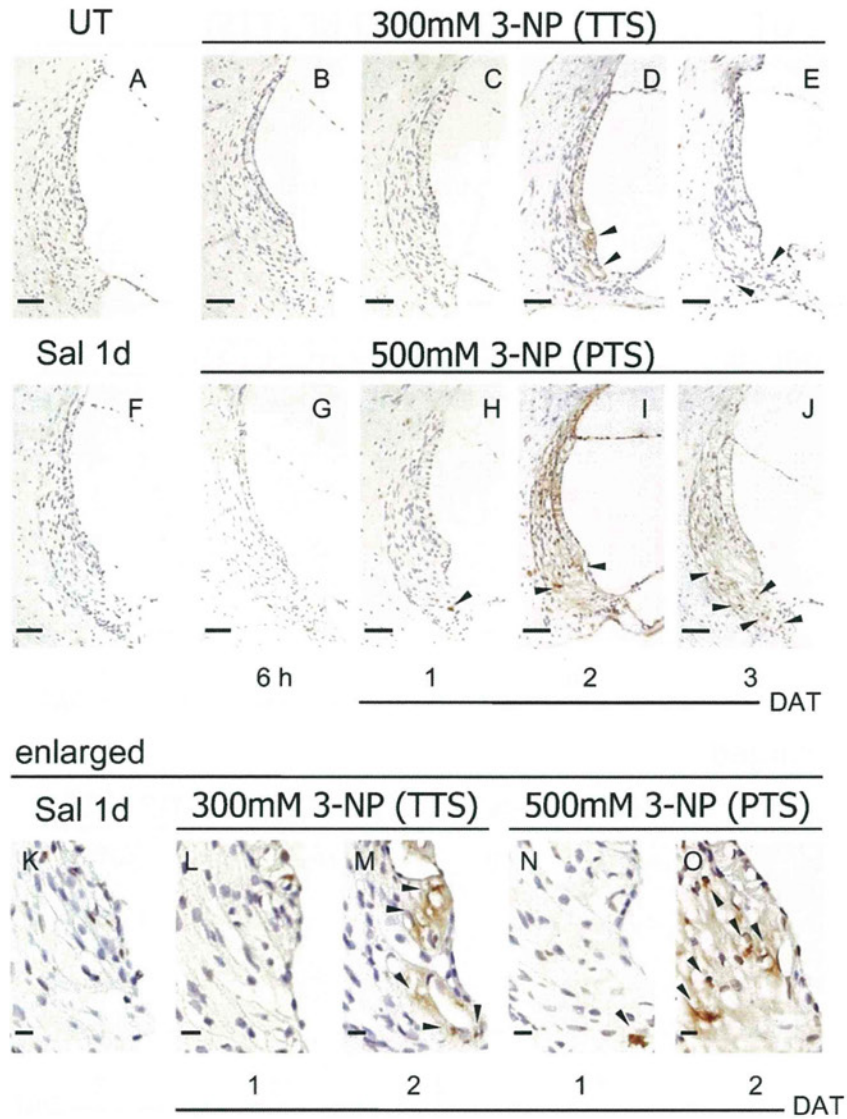

Fig. 4. TUNEL histochemical analysis of apoptotic cells in the LW after 3-NP treatment. Apoptotic cells were not detected in untreated control rats (UT; A) or in saline-treated rats (Sal 1d; F). In TTS rats treated with 300 mM 3-NP (B–E), a small number of apoptotic cells (arrowheads) were found at 2 DAT and 3 DAT (D, E). In PTS rats treated with 500 mM 3-NP (G–J), apoptotic cells were detectable at 1 DAT (H). The number of apoptotic cells (arrowheads) increased as the degenerating area expanded at 2 DAT and 3 DAT (I, J). K–O are enlarged images of spiral prominence of F, C, D, H and I, respectively. Scale bar = 50 μm (A–J) and 10 μm (K–O).

treated with 3-NP, because multiple attempts failed to show significant up-regulation of the ER stress mediators *grp78* and *grp94*. These results suggest that either a partial ER stress-response pathway including ATF-4 and CHOP is activated, or that mechanisms other than ER stress are responsible for the activation of the two molecules in the LW treated with 3-NP. CHOP has been reported to be induced without activation of other ER stress-responsive proteins such as GRP78 in a cultural experimental model of mitochondrial stress (Zhao et al., 2002). In this model, accumulation of unfolded proteins in the mitochondria resulted in induction of CHOP and mitochondrial molecular chaperones (e.g., Cpn60, Cpn10 and mtDnaJ), but did not induce non-mitochondrial chaperones including GRP78. Moisoi et al. (2009) also reported that *chop* expression was increased by mitochondrial dysfunction in the brain. Similarly, induction of *atf-4* and *chop* in the LW after 3-NP treatment may also be caused by mitochondrial stress following oxidative stress. On the other hand, investigation of PERK, IRE-1 and ATF-6 is necessary to demonstrate that ER stress is concerned with the increase of *chop* expression in this study.

The expression levels of *chop* at 6 h after 3-NP treatment and at 1 DAT were not significantly different between TTS and PTS rats, despite the contrasting number of degenerating cells at 3 DAT. Immunohistochemical study revealed nuclear staining of CHOP, which is required to undergo functional role for transcription factor, in PTS rats but rarely in TTS rats. This may explain the different levels of apoptosis at 3 DAT. Another possibility is that CHOP may be involved in the only initial induction of apoptosis in this model and another death pathway which sustained ongoing cell death was also activated in PTS rats but not activated in TTS rats. Further study to identify regulators of degeneration in LW fibrocytes will provide us with insight to develop strategies to prevent death of LW fibrocytes.

In summary, we characterized a novel molecular mechanism of acute hearing loss caused by 3-NP administration and identified CHOP, a mediator of oxidative stress, ER stress, and mitochondrial stress, as a preceding marker of damage in LW fibrocytes.

4. Experimental procedures

4.1. Animals and drug administration

Male Sprague–Dawley rats (6–8 weeks old, weighing 170–230 g) were used. The rats were housed in metallic breeding cages in a room with a light/dark

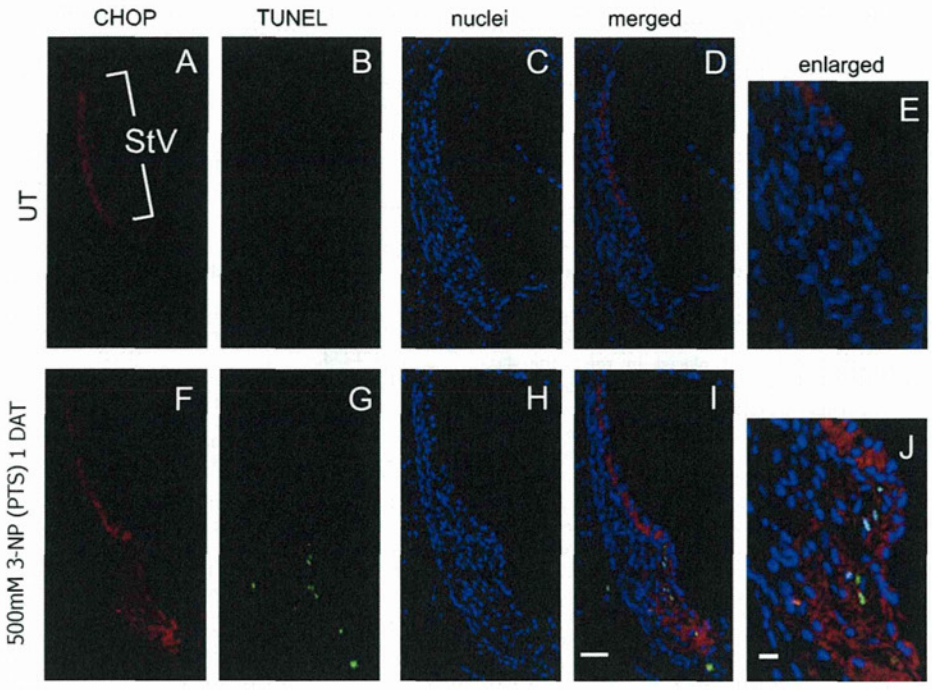

Fig. 5. Concurrent detection of CHOP and apoptosis in the LW after 3-NP treatment. The LW of untreated control rats (UT; A–E) and PTS rats treated with 500 mM 3-NP (F–J) were double-immunostained with antibodies to CHOP (red) and TUNEL (green), and counterstained with DAPI for nuclear staining (blue). Although apoptotic cells were not observed in untreated rats (B, D, and E), apoptosis was detected in the area of type II and type IV fibrocytes in PTS rats 1 day after 3-NP treatment (PTS rats 1 DAT; G) where the CHOP signal was enhanced (F, I, J). E and J were enlarged images of spiral prominence of D and H, respectively. StV; stria vascularis. Scale bar = 50 μm (A–D, F–I) and 10 μm (E, J). (For interpretation of the references to color in this figure legend, the reader is referred to the web version of the article.)

Table 1
PCR primers and their target genes used in the study.

Gene	Acc. number	Sequence (5′ > 3′)		Product length (bp)	Annealing temperature (°C)
		Forward	Reverse		
chop	U30186	AGTCTCTGCCTTTCGCCTTT	GCCACTTTCCTCTCATTCTC	382	55.4
atf-4	NM_024403	GCTGCCCCCTTTACATTCTT	AGCACAAAGCACCTGACTAC	615	54.5
grp78	XM_213908	AACGACCCCTGACAAAAGAC	TAGCCAATTCCTCCTCTCCC	768	57.9
grp94	XM_343192	ACACGGCTTGCTAAACTTCT	CTCTGGCTCTTCCTCTACCT	771	54.2
gapdh	M17701	GCCAAAAGGGTCATCATCTC	GCCTCTCTCTTGCTCTCAGT	715	55.5

Abbreviations: Acc. number: accession number; *chop*: C/EBP homologous protein; *atf-4*: activating transcription factor-4; *grp78* and *grp94*: glucose-regulated protein 78 and 94; *gapdh*: glyceraldehyde-3-phosphate dehydrogenase.

cycle of 12 h and humidity of 55% at 23 °C, with free access to food and water for at least 7 days before use. In these rats, hearing loss was induced by surgical administration of different concentrations of 3-NP onto the inner ear (Hoya et al., 2004). Before surgery, the rats were anesthetized with pentobarbital (40–50 mg/kg, i.p.) or pentobarbital (20–25 mg/kg, i.p.), ketamine (40–60 mg/kg, i.p.) and xylazine (4–6 mg/kg, i.p.). An incision was made posterior to the left pinna near the external meatus after local administration of lidocaine (1%). The left otic bulla was opened to approach the round window niche. The tip of a polyethylene tube (PE10, Becton Dickinson & Co., Franklin Lakes, NJ) was drawn to a fine tip in a flame and gently inserted into the round window niche. 3-NP (Sigma, St. Louis, MO) was dissolved in saline at 300 mM or 500 mM and the pH was adjusted to 7.4 with NaOH. Each 3-NP solution (3 μL) was administered with a syringe pump. Following 3-NP treatment, a tiny piece of gelatin was placed on the niche to keep the solution in the niche during head movement after awakening from anesthesia, and the wound was closed (Hoya et al., 2004; Okamoto et al., 2005). All the experimental procedures were performed in accordance with guidelines from the National Tokyo Medical Center, and were approved by the Animal Care and Use Committee of the Institute. Adequate measures were taken to minimize pain or discomfort of experimental animals.

4.2. Measurement of auditory brainstem response

ABRs were recorded from each rat before 3-NP treatment, and 3 h, 6 h, 1, 2, 3 and 7 days after 3-NP treatment. Pure tone bursts of 8 kHz and 20 kHz (0.2 ms rise/fall time 1 ms flat segment) were used, and auditory thresholds in the treated ear were measured at the same time point using incremental steps of 5 dB. Details of ABR recording were previously described (Hoya et al., 2004).

4.3. Semi-quantitative reverse transcription PCR

After the rats were anesthetized from each rat before 3-NP treatment, and 3 h, 6 h, 1, 2, 3 and 7 days after 3-NP treatment ($n = 5$), temporal bones were quickly removed and immersed in RNA later (Takara Bio, Shiga, Japan) on ice, followed by dissection of the middle turn of the LW. Total RNA was isolated using TRIzol reagent (cultural gen, Carlsbad, CA) according to the manufacturer's protocol. Total RNA was extracted by DEPC-treated water and the purity of total RNA was measured with a UV/visible spectrophotometer (Ultrospec 2100 pro; Amersham Pharmacia Biotech, Piscataway, NJ) by the ratio of OD_{260}/OD_{280}. First-strand cDNA synthesis was performed using 100 ng of total RNA and oligo$(dT)_{12-18}$ primers in a total volume of 20 μL according to the SuperScript III RNase H^- Reverse Transcriptase protocol (cultural gen). We used PCR primers specific for *chop*, *atf-4*, glucose-regulated protein *grp78* and *grp94*, and *gapdh*. The sequences of the PCR primers, sizes of the predicted PCR products, and the annealing temperature are listed in Table 1. The target genes were amplified in 25 μL of reaction containing 2.5 μL of diluted cDNA, 0.2 μM of each dNTP, 0.4 μM of each primer, 0.625 U of Taq DNA polymerase (Sigma) and 1 × buffer (10 mM Tris–HCl (pH 8.3), 50 mM KCl, 1.5 mM $MgCl_2$ and 0.001% gelatin). PCR was conducted at 94 °C for 5 min, 30 cycles of 94 °C for 1 min, the specific annealing temperature for 1 min, and 72 °C for 2 min, followed by 72 °C for 10 min, and then 10 μL of each PCR product was analyzed by 1% agarose gel electrophoresis in Tris–acetate-EDTA buffer. PCR products were electrophoresed and visualized using ethidium bromide. The images were captured by CS Analyzer (Atto, Tokyo, Japan).

4.4. Quantitative real-time RT-PCR analysis

qPCR was performed according to manufacturer's protocols for the ABI PRISM 7000 Sequence Detection System (Applied Biosystems, Foster City, CA). The